The Mitochondrial Permeability Transition Pore Activates a Maladaptive Mitochondrial Unfolded Protein Response

Suzanne Angeli[1*], Anna C. Foulger[1], Tanuja Harshani Peiris[1], Akos A. Gerencser[1], Manish Chamoli[1], Dipa Bhaumik[1], Azar Asadi Shahmirzadi[1,2], Julie K. Andersen[1,2*], Gordon J. Lithgow[1,2*]

[1]Buck Institute for Research on Aging; Novato, California, 94945 USA
[2]USC Leonard Davis School of Gerontology, University of Southern California, Los Angeles, California, 90191

*Correspondence: sangeli@buckinstitute.org, glithgow@buckinstitute.org, jandersen@buckinstitute.org

SUMMARY

Mitochondrial activity determines aging rate and the onset of chronic diseases. The mitochondrial permeability transition pore (mPTP) is a pathological pore in the inner mitochondrial membrane thought to be composed of the F-ATP synthase (complex V). Oligomycin sensitivity-conferring protein (OSCP), a subunit of F-ATP synthase, helps protect against mPTP formation. How the destabilization of OSCP may contribute to aging, however, is unclear. We have found that loss OSCP in the nematode *Caenorhabditis elegans* initiates the mPTP and shortens lifespan specifically during adulthood, in part via initiation of the mitochondrial unfolded protein response (UPR^mt). Genetic or pharmacological inhibition of the mPTP inhibits the UPR^mt and restores normal lifespan. The mitochondria of long-lived mutants are buffered from the maladaptive UPR^mt, partially via the transcription factor FOXO3a/*daf-16*. Our findings reveal how the mPTP/UPR^mt nexus may contribute to aging and age-related diseases and how inhibition of the UPR^mt may be protective under certain conditions.

INTRODUCTION

As mitochondrial function declines with age, the frequency of the mPTP increases (Rottenberg and Hoek, 2017). The mPTP is central to early-stage pathologies associated with several age-related diseases, including Alzheimer's and Parkinson's disease (AD, PD) and late-stage pathologies of ischemia-reperfusion injuries including heart attack and stroke (Ong et al., 2015; Panel et al., 2018). The mPTP is a pathological channel that forms in the inner mitochondrial membrane in response to excessive cytosolic Ca^{2+} or high ROS conditions. Sustained opening of the mPTP leads to outer mitochondrial membrane rupture, release of Ca^{2+} into the cytosol, and cell death (Bernardi and Di Lisa, 2015). Cyclosporine A (CysA), a well-characterized mPTP inhibitor, inhibits the mPTP by binding and sequestering cyclophilin D, a mitochondrially-localized peptidyl prolyl isomerase that helps catalyze pore formation (Basso et al., 2005; Nakagawa et al., 2005). Genetic inhibition of cyclophilin D protects against mPTP formation (Baines et al., 2005). The mPTP is also modulated by adenine nucleotide translocases (ANTs), which exchange ADP and ATP across the IMM. Genetic inhibition of ANTs also help prevent pore formation (Karch et al., 2019; Kokoszka et al., 2004). Both CysA and loss of ANTs have been shown to extend lifespan in *C. elegans* (Farina et al., 2008; Ye et al., 2014). Thus, the mPTP appears to be an important modulator of healthspan and lifespan.

Though the identification of the proteins that make up the mPTP is controversial, recent studies have pointed to F-ATP synthase (complex V) as the most probable candidate due to its ability to bind cyclophilin D and form Ca^{2+} currents.(Bernardi and Di Lisa, 2015; Mnatsakanyan and Jonas, 2020). Some models posit that dimeric forms of F-ATP synthase open to form a pore while other models have suggested that the pore occurs via the membrane-bound proton rotor (Alavian et al., 2014; Azarashvili et al., 2014; Bonora et al., 2013; Bonora et al., 2017; Giorgio et al., 2013; Mnatsakanyan et al., 2019; Neginskaya et al., 2019; Urbani et al., 2019). ATP5O, also known as oligomycin sensitivity-conferring protein (OSCP), a subunit of the F-ATP synthase that regulates ATPase rotational activity to provide efficient ATP production (Murphy et al., 2019), has emerged as an important regulator of the mPTP. OSCP levels decrease with normal aging and loss of OSCP increases propensity for pore formation *in vitro* and in mouse models of AD (Beck et al., 2016b; Gauba et al., 2017; Giorgio et al., 2013). Conversely, OSCP confers protection against the pore under low pH conditions and OSCP overexpression protects from mPTP initiation in AD and cardiac dysfunction models (Antoniel et al., 2018; Beck et al., 2016b; Guo et al., 2020). Thus, OSCP appears to be an important regulator of aging and disease progression, possibly via its ability to modulate mPTP formation.

Under stress, the mitochondria attempt to repair the damage, recycle damaged mitochondria, or, under deleterious circumstances, initiate cell death. Similar to the endoplasmic reticulum unfolded protein response (UPR^ER) and the cytoplasmic heat shock response (HSR), the mitochondrial unfolded protein response (UPR^mt) is capable of initiating a broad-range transcriptional response that, among other functions, aids in the refolding of mitochondrial matrix proteins (Naresh and Haynes, 2019). Recent studies also show that a loss of mitochondrial membrane potential correlates with activation of the UPR^mt, and disruption of mitochondrial processes other than protein misfolding, such as those involved in TCA cycle and lipid catabolism, also induce the UPR^mt (Rolland et al., 2019). UPR^mt activation is associated with longevity and improvement in neurodegenerative models (Durieux et al., 2011; Houtkooper et al., 2013; Kim et al., 2016; Merkwirth et al., 2016; Sorrentino et al., 2017; Tian et al., 2016), but it has also conversely been shown to increase neurodegeneration, propagate mtDNA mutations, and exacerbate ischemic conditions (Lin et al., 2016; Martinez et al., 2017; Yung et al., 2019), underscoring its complexity. If left unmitigated, UPRs can initiate cell death (Iurlaro and Munoz-Pinedo, 2016; Munch and Harper, 2016). Thus, the context or cellular environment are important determinants of whether UPR^mt induction results in beneficial or detrimental effects.

In *C. elegans*, mild mitochondrial perturbations early in life can extend lifespan. Loss of OSCP/*atp-3* has previously been shown to extend lifespan when initiated during larval development (Dillin et al., 2002; Rea et al., 2007). In contrast, here, we have determined that loss of OSCP/*atp-3* during adulthood leads to initiation of the mPTP, the UPR^mt, and a shortened lifespan. Surprisingly, *atfs-1*, the UPR^mt master transcription factor (Haynes et al., 2010; Nargund et al., 2012), helps drive the reduction of lifespan, suggesting that the UPR^mt program promotes aging during adulthood. The adult UPR^mt is responsive to mPTP regulators, including the immunosuppressive drug, CysA, as well as a mitochondrially-localized cyclophilin and ANTs, pointing to a previously undiscovered coordination between the UPR^mt and the mPTP. We find that proton rotor subunits as well as subunits important for dimerization of the F-ATP synthase are essential for transducing the adult UPR^mt. Loss of these subunits as well as pharmacological CysA treatment restores lifespan due to loss of OSCP/*atp-3*. These results are

consistent with current models that posit that the F-ATP synthase forms the mPTP (Bernardi and Di Lisa, 2015). Remarkably, we find that long-lived mutants which have previously been shown to be protected from the mPTP (Zhou et al., 2019) expressing high FOXO3a/*daf-16* activity do not initiate a UPR^{mt} during adulthood. Overall, our findings point to a model in which loss of OSCP/*atp-3* in adults induces mPTP formation and subsequent detrimental activation of the UPR^{mt}, from which long-lived mutants are buttressed. Understanding the relationship between these two mitochondrial processes will undoubtedly further our understanding of aging as well as disparate age-related disorders, including neurodegenerative diseases, cancer, heart-attack, and stroke.

RESULTS

Loss of OSCP/*atp-3* Induces Mitochondrial Permeability Transition Pore (mPTP) Characteristics

The opening of the mPTP is characterized by a loss of membrane potential as well as an increase in cytosolic Ca^{2+}. We observed that a reduction in the abundance of OSCP/*atp-3* by RNA interference (RNAi) caused a loss of membrane potential as measured by the mitochondrial dye, TMRM, in young adult worms (Figure 1A, 1B). Strikingly, RNAi of other OXPHOS subunits from complex I, IV, and V had no effect on membrane potential. RNAi of OSCP/*atp-3* during adulthood also caused an increase in cytosolic Ca^{2+} as measured by the intestinal FRET-based Ca^{2+} reporter, KWN190, while RNAi of other F-ATP synthase subunits, F6/*atp-4* and d/*atp-5*, did not (Figure 1C). Loss of OSCP/*atp-3* also induced mitochondrial swelling and fragmentation (Figure 1D, 1E). In contrast, we observed no swelling or fragmentation following the reduction in expression of the F-ATP synthase subunit d/*atp-5* (Figure 1F). These results suggest that loss of OSCP/*atp-3* during adulthood uniquely induces the mPTP in *C. elegans*.

To verify the stability of the mitochondrial membrane potential after RNAi of other OXPHOS subunits, we checked for RNAi efficiency via qPCR; we observed efficient mRNA reduction from subunit *cco-1* from complex IV as well as from several of the complex V subunits, including *atp-1*, *atp-2*, *atp-4*, and *atp-5* (Figure S1A-S1E). We also examined protein levels for subunits in which antibodies were available and observed that RNAi of the complex I subunit NUO-2 and complex V subunits ATP-1 and ATP-2 resulted in significant knockdown of protein levels (Figure S1F-S1H). These findings show that knockdown of OXPHOS subunits other than OSCP/*atp-3* do not lead to a loss of membrane potential.

Loss of OSCP/*atp-3* Induces a Unique UPR^{mt} During Adulthood

A recent study showed that a loss of membrane potential is associated with inducing the UPR^{mt} (Rolland et al., 2019). To determine if loss of OSCP/*atp-3* selectively induces the UPR^{mt} during adulthood due to the observed drop in membrane potential, we utilized a GFP reporter under the promoter of the mitochondrial UPR chaperone, *hsp-6* (p*hsp-6*::GFP) (Yoneda et al., 2004) and compared it to select representative OXPHOS genes encoding complex I, III, IV, and V subunits. RNAi of OXPHOS subunits induced little to no UPR^{mt} if initiated after the last larval stage (L4), which we termed the post-developmental UPR^{mt} (pdvUPR^{mt}). Only RNAi of OSCP/*atp-3* induced a robust UPR^{mt} in young adults (Figure 2A, 2B, Table S1), the timing of which corresponded with the drop in membrane potential (Figure 1A, 1B). In contrast, RNAi of all same genes induced a robust UPR^{mt} if initiated during the early larval stages (L1, L2, and L3) of
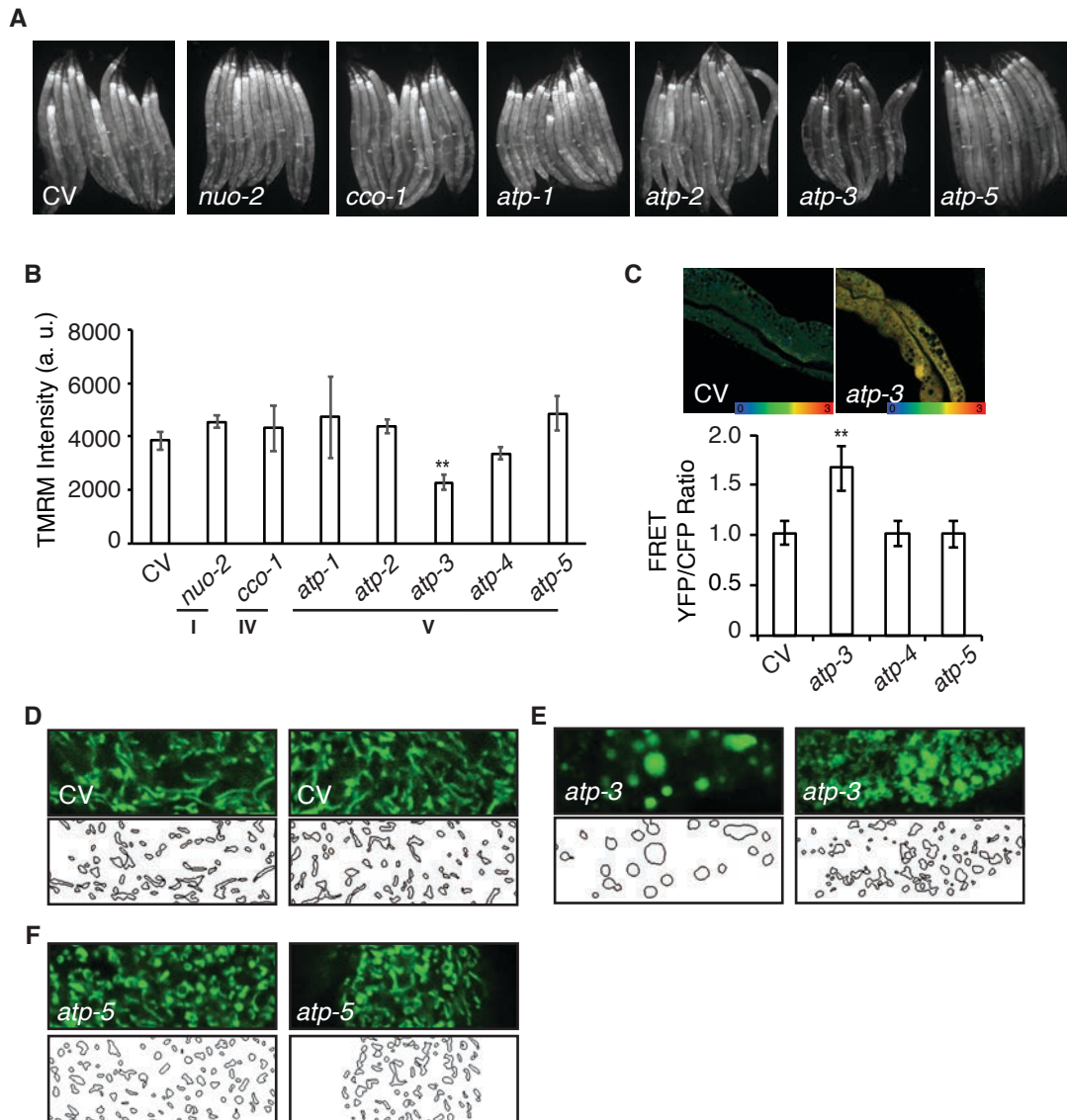
Figure 1: Loss of OSCP/*atp-3* Selectively Recapitulates mPTP-like Characteristics

(A) RNAi of various OXPHOS subunits in N2 wild-type worms did not lead to changes in the membrane potential as measured by the TMRM dye, except for RNAi of OSCP/*atp-3*. RNAi was administered for 48 hours beginning at young adulthood. TMRM was administered via the NGM plates.

(B) Quantification of TMRM intensity from (A). Data are the mean ± SEM of ≤ 15 animals combined from three biological experiments. **$p \leq 0.01$ by Student's *t*-test. I, IV, and V correspond to OXPHOS complexes.

(C) RNAi of OSCP/*atp-3* leads to an increase in cytosolic calcium as measured by the FRET-based calcium indicator protein D3cpv/cameleon. RNAi was administered for 48 hours beginning at young adulthood. Data are the mean ± SEM of ≤ 15 animals combined from three biological experiments. **$p \leq .01$ by Student's *t*-test.

(D-F) Confocal micrographs of intestinal mitochondria labeled with GFP (p*ges-1*::GFP^mt) in young adults. RNAi and was administered for 48 hours beginning at young adulthood, then worms were removed from the RNAi and aged until Day 7 of adulthood followed by collection for microscopy. Top panels, fluorescent channel; bottom panels, rendering of individual mitochondria. See Materials and Methods for details on rendering.

4

development (dvUPR^{mt}) (Figure 2A, 2B).These results are consistent with previous reports demonstrating that the UPR^{mt} is robustly induced during development but poorly induced during adulthood in *C. elegans* (Durieux et al., 2011; Labbadia and Morimoto, 2015). Loss of membrane potential *per se* via FCCP, a potent mitochondrial uncoupler, however, did not induce a UPR^{mt} in young adults, suggesting that uncoupling and its associated loss in membrane potential is not sufficient to induce a pdvUPR^{mt} (Figure S1I). Post-developmental loss of OSCP/*atp-3* increased endogenous transcript levels of *hsp-6* as well as endogenous HSP-6/mtHSP70 protein levels (Figure S2A, S2B). Post-developmental loss of OSCP/*atp-3* mildly induced the mitochondrial chaperone reporter p*hsp-60::*GFP (Figure S2C, S2D). Neither the UPR^{ER} nor the HSR were induced by post-developmental loss of OSCP/*atp-3* (Figure S2C). RNAi of other mitochondrial genes that are known to induce a dvUPR^{mt}, *clk-1* (coenzyme Q hydroxylase), *mrps-5* (mitochondrial ribosome), and *tomm-22* (translocase of outer mitochondrial membrane) (Baker et al., 2012; Bennett et al., 2014; Houtkooper et al., 2013), did not induce the pdvUPR^{mt} (Table S1). Importantly, we found that the pdvUPR^{mt} was dependent on the master UPR^{mt} transcription factor, *atfs-1*, as well as its previously described co-factors, the peptide exporter *haf-1* and the ubiquitin-like protein *ubl-5* (Figure 2C, 2D) (Haynes et al., 2010), demonstrating that the pdvUPR^{mt} is regulated similarly to the previously described dvUPR^{mt}. Thus, loss of OSCP/*atp-3* induces a robust and specific pdvUPR^{mt} which is dependent on the conserved transcription factor ATFS-1.

The Post-Developmental UPR^{mt} is Temporally Confined and Reversible
Given that the UPR^{mt} has been studied during development in *C. elegans,* we sought to determine the window of the UPR^{mt} during adulthood. We initiated RNAi of OSCP/*atp-3* beginning at the last larval stage (L4 stage) and every few hours thereafter into adulthood. GFP expression was examined 48 hours after RNAi initiation (Figure S2E). We observed that the pdvUPR^{mt} is initiated up to 6 hours after the L4 stage, after which RNAi of OSCP/*atp-3* no longer induced the UPR^{mt}. In contrast, RNAi of COX5B/*cco-1* of complex IV had no effects on the UPR^{mt} at any of these stages (Figure S2E). For all subsequent post-development experiments, RNAi was therefore administered at the young adult stage corresponding to 4-hours after the L4 stage. Thus, the pdvUPR^{mt} is confined to pre-gravid stages of adulthood, corresponding with previous reports showing a global decline in stress responses at the onset of egg-laying (Labbadia and Morimoto, 2015).

Previous studies have shown that developmental RNAi of *cco-1* RNAi leads to persistent activation of the UPR^{mt} into adulthood, even after removal from RNAi (Durieux et al., 2011). Similarly, we observed that developmental RNAi of OSCP/*atp-3* initiated a UPR^{mt} that persisted into adulthood, even after removal from *atp-3* RNAi (Figure S2F). In contrast, removal from post-developmental *atp-3* RNAi treatment led to a steady decline in the GFP signal (Figure S2F), suggesting the activation of the pdvUPR^{mt} is reversible.

Loss of ATP Synthase ATPases Induce a Post-Developmental UPR^{mt}
F-ATP synthase is composed of a membrane-bound proton rotor (Fo), a catalytic ATPase that converts ADP to ATP (F1), and peripheral stalk and supernumerary subunits that help bridge these two portions together (Figure 2F). OSCP/*atp*-3 sits atop the ATPase and helps tether it to the peripheral stalk subunits. We systematically tested via RNAi whether loss of F-ATP synthase subunits other than OSCP/*atp-3* could induce a pdvUPR^{mt}. During adulthood, loss of rotor
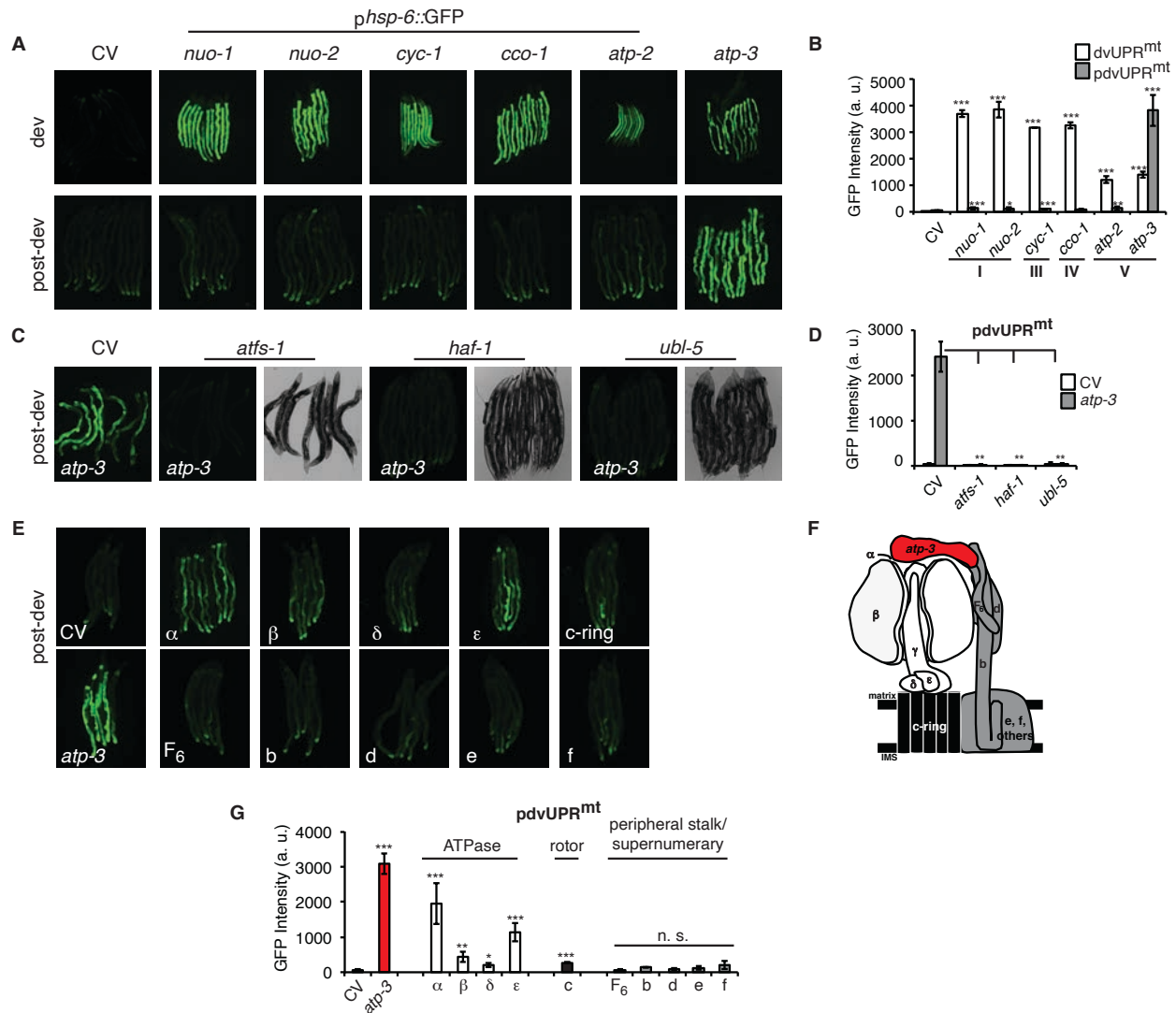
Figure 2: Loss of OSCP/*atp-3* and ATPases Initiate a Post-developmental UPR[mt]

(A) Developmental RNAi of OXPHOS subunits induced the p*hsp-6*::GFP reporter while only OSCP/*atp-3* RNAi induced the reporter when initiated during post-development. For developmental treatment, worms were exposed to RNAi beginning from eggs for 72 hours. For post-developmental treatment, worms were exposed to RNAi beginning from young adulthood for 48 hours. CV, control vector RNAi; dev, development; post-dev, post-development.

(B) Quantification of GFP intensity from (A). Data are the mean ± SEM of ≤ 15 animals combined from three biological experiments. *p ≤ 0.05, **p ≤ 0.01, and ***p ≤ .0001 by Student's *t*-test. dv, development; pdv, post-development; I, III, IV, and V correspond to OXPHOS complexes I-V.

(C) Post-developmental RNAi of OSCP/*atp-3* induced the p*hsp-6*::GFP reporter, which is abrogated via co-treatment with *atfs-1*, *haf-1*, or *ubl-5* RNAi. Worms were exposed to RNAi beginning from young adulthood for 48 hours. Left panels, fluorescent channel; right panels, bright-field channel. CV, control vector RNAi; post-dev, post-development.

(D) Quantification of GFP intensity from (C). Data are the mean ± SEM of ≤ 15 animals combined from three biological experiments. **p ≤ 0.01 by Student's *t*-test. pdv, post-development.

(E) Post-developmental RNAi of ATPase and c-ring subunits but not peripheral stalk or supernumerary subunits of the F-ATP synthase induced the p*hsp-6*::GFP reporter. Worms were exposed to RNAi beginning from young adulthood for 48 hours. post-dev, post-development.

(F) Schematic of monomeric F-ATP synthase. White subunits, ATPase; black subunits, H+-rotor/c-ring; grey subunits, peripheral stalk and supernumerary subunits; red subunit, oligomycin sensitivity-conferring protein (OSCP/*atp-3*).

(G) Quantification of GFP intensity from (E). Data are the mean ± SEM of ≤ 15 animals combined from three biological experiments. *p ≤ 0.05, **p ≤ 0.01, and ***p ≤ .0001 by Student's *t*-test. pdv, post-development.

6

subunits (c-ring/*Y82E9BR.3*), peripheral stalk or supernumerary subunits (F6/*atp-4*, d/*atp-5*, b/*asb-2*, e/*R04F11.2*, f/*R53.4*), induced little to no UPR^{mt} (Figure 2E, 2G, Table S2). Loss of the ATPase subunits (α/*atp-1*; β/*atp-2*; δ/*F58F12.1*; ϵ/*hpo-18*) induced a mild to moderate UPR^{mt}, though none as robustly as loss of OSCP/*atp-3*. Subunits α and ϵ induced a moderate UPR^{mt}, while loss of the β and δ subunits induced a limited, though significant, UPR^{mt} (Figure 2E, 2G, Table S2). In contrast, during development, loss of rotor subunits, ATPase subunits, or peripheral stalk and supernumerary subunits all induced a robust UPR^{mt} (Figure S2G, S2H). Thus, in addition to the robust induction of the pdvUPR^{mt} caused by loss of OSCP/*atp-3*, loss of F-ATP synthase ATPases moderately to mildly induce the pdvUPR^{mt}.

The Post-Developmental UPR^{mt} is dependent on Mitochondrial Permeability Transition Pore (mPTP) Factors

To determine if the pdvUPR^{mt} is initiated in response to the mPTP, we tested pharmacological and genetic modulators of the mPTP on induction of the pdvUPR^{mt}. The mPTP is known to be inhibited by the immunosuppressive drug, cyclosporin A (CysA). CysA binds cyclophilins, which in the cytoplasm regulates calcineurin signaling (Liu et al., 1991; Takahashi et al., 1989), while in the mitochondria inhibits the mPTP (Nicolli et al., 1996). To parse out the mitochondrial versus cytoplasmic functions of CysA, we also tested the cytoplasmic-only immunosuppressive drug, FK506, which acts similarly to CysA in that it modulates calcineurin signaling in the cytoplasm (Liu et al., 1991). We observed that CysA strongly inhibited the pdvUPR^{mt} but not dvUPR^{mt} in a dose-dependent manner (Figure 3A, 3B, Figure S3A). In contrast, we found that FK506 had no effect on the pdvUPR^{mt} (Figure 3A, 3B, Figure S3B), demonstrating that CysA acts in the mitochondria to suppress the pdvUPR^{mt}. The mPTP has been shown to be regulated by adenine nucleotide translocases (ANTs) of the inner mitochondrial membrane and loss of ANTs helps prevent the mPTP (Karch et al., 2019). We tested *ant-1.1*, which is ubiquitously expressed in *C. elegans*, and *ant-1.2*, which is expressed predominantly in the pharynx and intestines (Farina et al., 2008). RNAi of *ant-1.1* moderately suppressed the pdvUPR^{mt} while RNAi of *ant-1.2* strongly suppressed the pdvUPR^{mt}, but not the dvUPR^{mt} (Figure 3C, 3D). In mammals, CysA acts in the mitochondria to inhibit the mPTP by binding and sequestering cyclophilin D, a peptidyl prolyl isomerase (Nicolli et al., 1996). *C. elegans* contains 17 poorly defined cyclophilins, of which 2 are predicted to be mitochondrially localized, *cyn-1* and *cyn-17* (Table S3). RNAi of *cyn-1* did not inhibit the pdvUPR^{mt} while *cyn-17* did (Figure 3D), suggesting that *cyn-17* may act similarly to cyclophilin D in mediating a conformation change that leads to the mPTP. RNAi of *cyn-17* did not affect the dvUPR^{mt} (Figure 3C). Together, these results show that the pdvUPR^{mt} is regulated by canonical pharmacological and genetic mPTP factors.

Loss of Essential F-ATP Synthase Subunits Important for the mPTP Suppress the Post-Developmental UPR^{mt}

Current models posit that the F-ATP synthase forms a pore that is capable of releasing Ca^{2+} under conditions of high oxidative stress, leading to rupturing of the mitochondria and initiation of cell death cascades. Some models suggest that ATP synthase dimers are required for the mPTP (Figure 3G) and that peripheral and supernumerary subunits are essential for pore formation (Carraro et al., 2014; Guo et al., 2019). Other models demonstrate that ATP synthase monomers (Figure 2F) are sufficient for the mPTP and specify the c-ring proton rotor as the
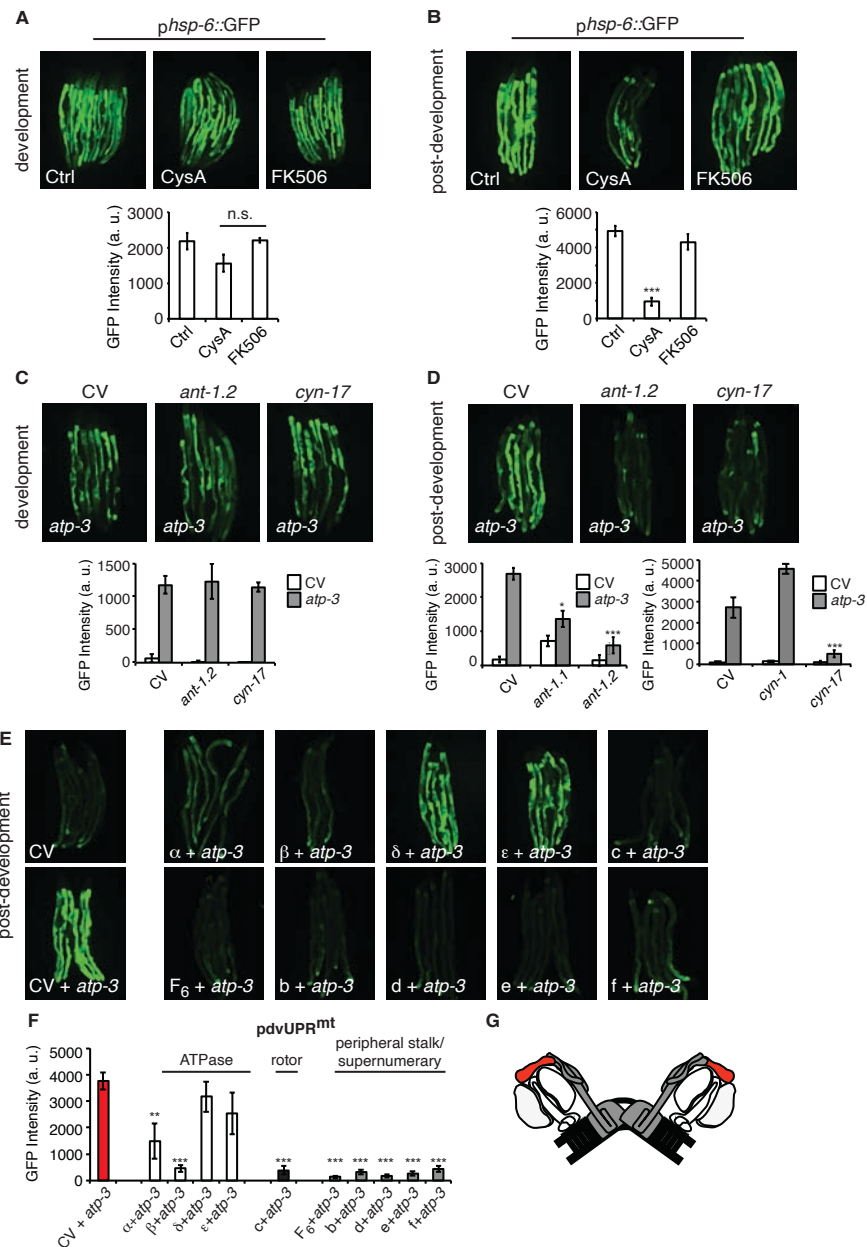
Figure 3: The Post-developmental UPR^{mt} is Regulated by Pharmacological and Genetic Modulators of the mPTP

(A, B) 15 μM of the immunosuppressants cyclosporin A (CysA) and FK506 had no effect on the dvUPR (A) but selectively suppressed the pdvUPR^{mt} in the p*hsp-6*::GFP reporter strain (B). Data are the mean ± SEM of ≤ 15 animals combined from three biological experiments. ***p ≤ .0001 by Student's *t*-test.

(C, D) Loss of cyclophilin *cyn-17* and adenine nucleotide translocase *ant-1.2* via RNAi had no effect on the dvUPR^{mt} (C) while their loss suppressed the pdvUPR^{mt} in the p*hsp-6*::GFP reporter strain (D). *ant-1.1* partially suppressed the pdvUPR^{mt} (D). Data are the mean ± SEM of ≤ 15 animals combined from three biological experiments. *p ≤ .05 , ***p ≤ .0001 by Student's *t*-test.

(E) Concomitant post-developmental RNAi of OSCP/*atp-3* and individual F-ATP synthase subunits inhibited the post-developmental UPR^{mt} to varying degrees.

(F) Quantification of GFP intensity from (E). Data are the mean ± SEM of ≤ 15 animals combined from three biological experiments. **p ≤ .001, ***p ≤ 0.0001 compared to CV + *atp-3* condition by Student's *t*-test. pdv, post-development.

(G) Schematic of ATP synthase dimers. White subunits, ATPase; black subunits, H+ rotor/c-ring; grey subunits, peripheral stalk and supernumerary subunits; red subunit, oligomycin sensitivity-conferring protein (OSCP/*atp-3*).

8

actual pore-forming component (Alavian et al., 2014; Azarashvili et al., 2014; Bonora et al., 2013; Bonora et al., 2017; Giorgio et al., 2013; Mnatsakanyan et al., 2019; Neginskaya et al., 2019; Urbani et al., 2019). To determine whether the structural integrity of F-ATP synthase subunits were required for the pdvUPR^{mt}, we systematically knocked down OSCP/*atp-3* as well as one additional F-ATP synthase subunit via RNAi. When we knocked down the c-ring subunits (color coded black) as well as peripheral and supernumerary subunits (color coded grey) via RNAi in adults, we observed nearly complete inhibition of the OSCP/*atp-3* RNAi-mediated pdvUPR^{mt} ((Figure 3E, 3F). When we knocked down the ATPase subunits in adults, we observed that loss of the β/*atp-2* subunit robustly suppressed the OSCP/*atp-3* RNAi-mediated pdvUPR^{mt}, possibly due to its role in modulating Ca^{2+} in the mPTP (Giorgio et al., 2017), while loss of α/*atp-1* moderately inhibited the pdvUPR^{mt} (Figure 3E, 3F, color coded white). Loss of the ATPase subunits δ/*F58F12.1* or ε/*hpo-18* in adults did not affect the pdvUPR^{mt}. In contrast, dual loss of subunits during development all robustly activated the dvUPR^{mt} (Figure S3C, S3E). Dual loss of subunits from other OXPHOS complexes (NDUFS3/*nuo-2*, complex I; COX5B/*cco-1*, complex IV) had no effect or slightly increased the dvUPR^{mt} and the pdvUPR^{mt} (Fig S3D, S3F). Thus, we find subunits critical for dimerization (peripheral and supernumerary subunits) and proton translocation (c-ring rotor) are required to transduce the OSCP/*atp-3* RNAi-mediated pdvUPR^{mt}. We also find that the β/*atp-2* subunit, previously found to play an important role in Ca^{2+} mediated mPTP, is required to transduce the OSCP/*atp-3* RNAi-mediated pdvUPR^{mt}. Taken together, these findings support a model in which inhibition of the mPTP via deletion of critical F-ATP synthase subunits inhibits the pdvUPR^{mt}.

Loss of OSCP/*atp-3* During Adulthood Promotes Aging Partially via the UPR^{mt}
Previous reports have shown that loss of OSCP/*atp-3* initiated during development robustly increases lifespan in *C. elegans* (Dillin et al., 2002), but how loss of OXPHOS subunits during adulthood affects lifespan has not been well studied. We initiated RNAi during both development and post-development. As previously reported, we found that developmental RNAi treatment led to lifespan extension (Figure 4A, Table S4). Worms continuously exposed to OSCP/*atp-3* RNAi during post-development experienced a high incidence of matricide (data not shown). To circumvent this outcome, we administered OSCP/*atp-3* RNAi to young adults for 48 hours of adulthood and observed approximately a 38% decrease in lifespan independent of matricide (Figure 4A, 4B, Table S4). Surprisingly, when *atfs-1* mutants were exposed to OSCP/*atp-3* RNAi during adulthood for 48 hours, we observed only about a 19% decrease in lifespan, suggesting that the initiation of the pdvUPR^{mt} via *atfs-1* contributes to reduced lifespan (Figure 4B, Table S4). Loss of other OXPHOS subunits had little or no effect on lifespan when administered during adulthood for 48 hours (Figure 4C, Table S4). Thus, we have determined that loss of OSCP/*atp-3* induces an age-accelerating, transcriptionally-dependent pdvUPR^{mt} not previously described in *C. elegans*.

Pharmacological or Genetic Inhibition of the mPTP Restores Lifespan
To determine if inhibition of the mPTP could also inhibit its associated toxicity, we tested the mPTP inhibitor, CysA, in lifespans. We found that CysA treatment was sufficient to rescue the shortened lifespan caused by RNAi of OSCP/*atp-3* in adults (Figure 4D). Based on our observations that loss of peripheral stalk subunits are capable of suppressing the pdvUPR^{mt}, we tested if their loss would also suppress the shortened lifespan. RNAi with either F6/*atp-4* or
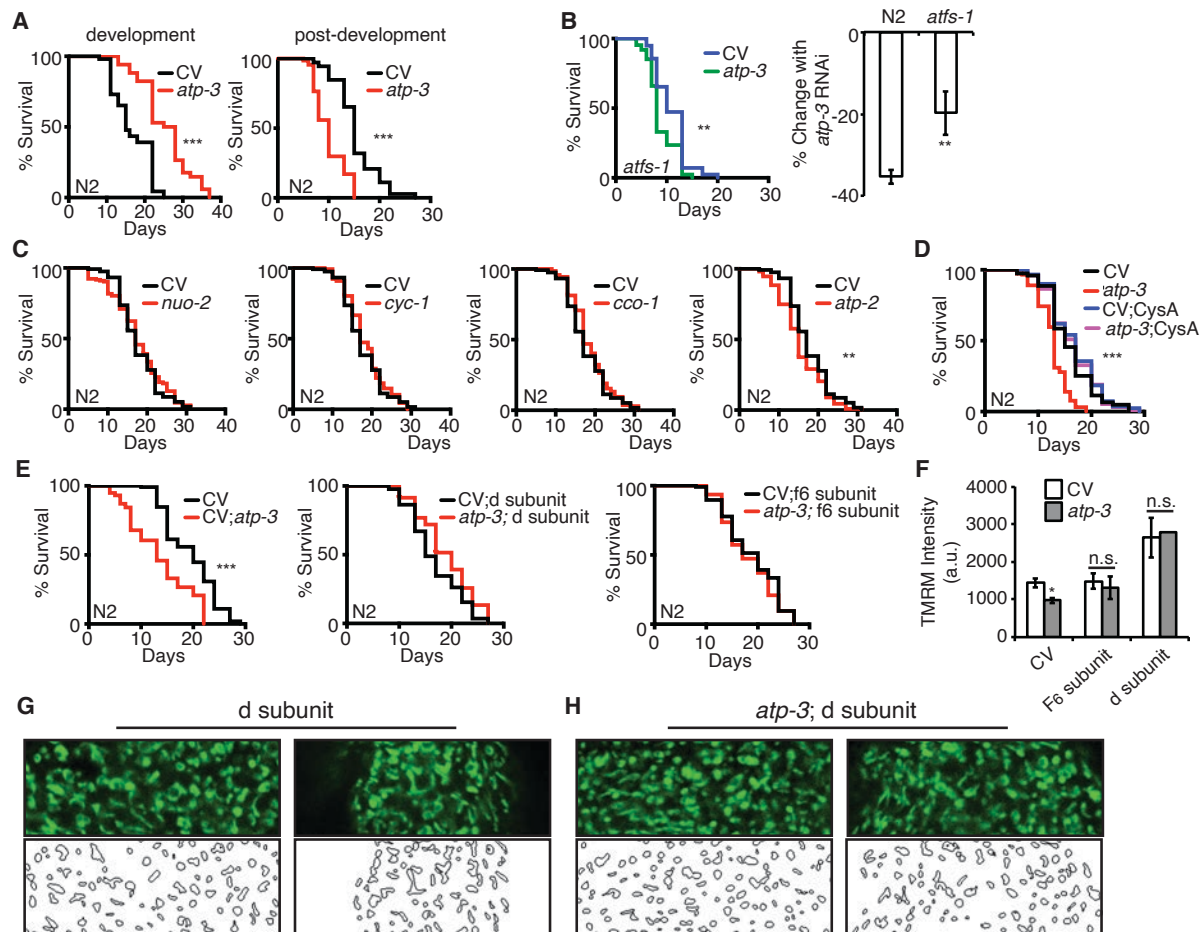
Figure 4: Loss of OSCP/*atp-3* Shortens Lifespan, which is Restored by Pharmacological or Genetic Inhibition of the mPTP

(A) Survival curves of wild-type N2 animals on CV or OSCP/*atp-3* RNAi initiated during development or post-development. Representative curves selected from three biological experiments. ***p ≤ .0001 by Log Rank (Mantel Cox). CV, control vector RNAi.

(B) Survival curves of *atfs-1(tm4525)* when OSCP/*atp-3* RNAi is initiated during post-development. Representative curves selected from three biological experiments. **p ≤ 0.01 by Log Rank (Mantel Cox). Bar graph is a quantification of percent change in lifespan of N2 or *atfs-1(tm4525)* mutant. **p ≤ 0.01 by Student's *t*-test is the mean of the percent change in lifespan ± SEM from three biological experiments. CV, control vector RNAi.

(C) Survival curves of wild-type N2 animals on indicated RNAi initiated during post-development. Representative curves selected from three biological experiments. **p ≤ 0.01 by Log Rank (Mantel Cox).

(D) Survival curves of wild-type N2 animals on CV or OSCP/*atp-3* RNAi initiated during post-development and treated with 15μM CysA. Lifespan curves from two pooled biological replicates, ***p ≤ .0001 by Log Rank (Mantel Cox) between CV and OSCP/*atp-3* RNAi. CV, control vector RNAi.

(E) Survival curves of wild-type N2 animals on CV or OSCP/*atp-3* RNAi with the additional loss of either F6 subunit/*atp-4* or d subunit/*atp-5* subunits via RNAi initiated during post-development. Lifespan curves from two pooled biological replicates, ***p ≤ .0001 by Log Rank (Mantel Cox). CV, control vector RNAi.

(F) Quantification of membrane potential as measured by TMRM after post-developmental RNAi of OSCP/*atp-3* with either F6 subunit/*atp-4* or d subunit/*atp-5* RNAi. Data are the mean ± SEM of ≤ 15 animals combined from three experiments. *p ≤ 0.05 by Student's *t*-test. CV, control vector RNAi.

(G, H) 63X confocal micrographs of intestinal mitochondrial GFP worms (p*ges-1*::GFP[mt]) treated with post-developmental dual-RNAi of d subunit/*atp-5* with CV or OSCP/*atp-3* RNAi. Top panel, fluorescent channel, bottom panels, rendering of individual mitochondria. See Materials and Methods for details on rendering.

10

d/*atp-5* rescued the shortened lifespan caused by RNAi of OSCP/*atp-3* in adults as well as restored the loss in membrane potential (Figure 4E, 4F). Loss of d/*atp-5* subunit also suppressed the mitochondrial swelling and fragmentation observed after OSCP/*atp-3* RNAi (Figure 4G, 4H). Thus, inhibition of key subunits of F-ATP synthase as well as pharmacological inhibition of the mPTP by CysA rescues the mPTP/pdvUPR^{mt} toxicity and rescues its effects on aging.

To verify that the use of dual-RNAi did not interfere with knockdown of OSCP/*atp-3*, we assessed an endogenously-expressing p*atp-3*::ATP-3::GFP translational reporter generated via CRISPR-Cas-9 (Figure S4A). We observed efficient knockdown of OSCP/*atp-3* via RNAi in the presence of either β/*atp-2* or d/*atp-5* RNAi, two subunits that suppress the pdvUPR^{mt}, demonstrate that the inhibition of the pdvUPR^{mt} is not due to ineffective RNAi of OSCP/*atp-3* but rather the functional consequences of removal of additional ATP synthase subunits. To examine the effects of dual-RNAi another way, we examined how loss of ATP synthase subunits impacted the pdvUPR^{mt} after α/*atp-1* RNAi, which induced the second most robust pdvUPR^{mt} (Figure 2E, 2G). Remarkably, we see the same pattern of pdvUPR^{mt} activation and inhibition as with loss of OSCP/*atp-3*: loss of the ATPase subunit β/*atp-2* and peripheral stalk subunit d/*atp-5* suppressed the α/*atp-1* RNAi-mediated pdvUPR^{mt} while loss of NDUFS3/*nuo-2* and COX5B/*cco-1* had no effect (Figure S4B). Importantly, immunoblots against α/*atp-1* showed similar protein knockdown under all conditions (Figure S4B), confirming that dual-RNAi is an effective method to assess the structural components of the F-ATP synthase.

Longevity Mutants Display Exceptional Mitochondria Partially via FOXO3a/*daf-16*
Given that the mPTP can accelerate aging, we tested whether long-lived worms, *glp-1(e2141)* (Notch-1 germline signaling), *daf-2(e1370)* (insulin/IGF-1-like signaling), and *eat-2(ad465)* (caloric restricting), were protected from the mPTP/pdvUPR^{mt}. We also included *fem-1(hc17)* (sperm deficient) mutants, which we identified as long-lived (Figure S5A, S5B). RNAi of OSCP/*atp-3* induced little to no pdvUPR^{mt} in *glp-1(e2141)*, *fem-1(hc17)*, and *daf-2(e1370)* backgrounds, while a moderate pdvUPR^{mt} was induced in *eat-2(ad465)* (Figure 5A, 5B). For simplicity, we next focus on the germline mutants, *fem-1(hc17)* and *glp-1(e2141)*. We found that *fem-1(hc17)* and *glp-1(e2141)* were able to induce a robust UPR^{mt} similar to control when RNAi was initiated during development (Figure S5C). The mutants also initiated a normal UPR^{ER} and heat shock response (HSR) during adulthood (Figures S5D-F). Thus, mutations that confer longevity specifically repress the pdvUPR^{mt}.

We next sought to determine the mechanism of suppression of the pdvUPR^{mt} by mutations conferring longevity. The longevity of *glp-1* and *daf-2* has previously been shown to be dependent on the transcription factor FOXO3A/*daf-16* (Hsin and Kenyon, 1999; Kenyon et al., 1993) and we also found that the longevity of *fem-1(hc17)* to be dependent on FOXO3a/*daf-16* (Figure S5A, S5B). On the other hand, *eat-2* has previously been found to be dependent on FOXA/*pha-4* (Panowski et al., 2007). Thus, we tested whether FOXO3a/*daf-16* was required for the suppression of the pdvUPR^{mt} and found that introducing the mutation, *daf-16(mu86)*, partially restored the pdvUPR^{mt} in *glp-1(e2141)* mutants and completely restored it in *fem-1(hc17)* mutants (Figure 5C). Previous studies have suggested that an increase in mitochondrial biogenesis may protect against opening of the mPTP (Goncalves et al., 2016). To determine if *fem-1(hc17)* and *glp-1(e2141)* exhibited enhanced mitochondrial content via FOXO3a/*daf-16*, we examined the mitochondria in the intestines where the UPR^{mt} is most robustly activated. We
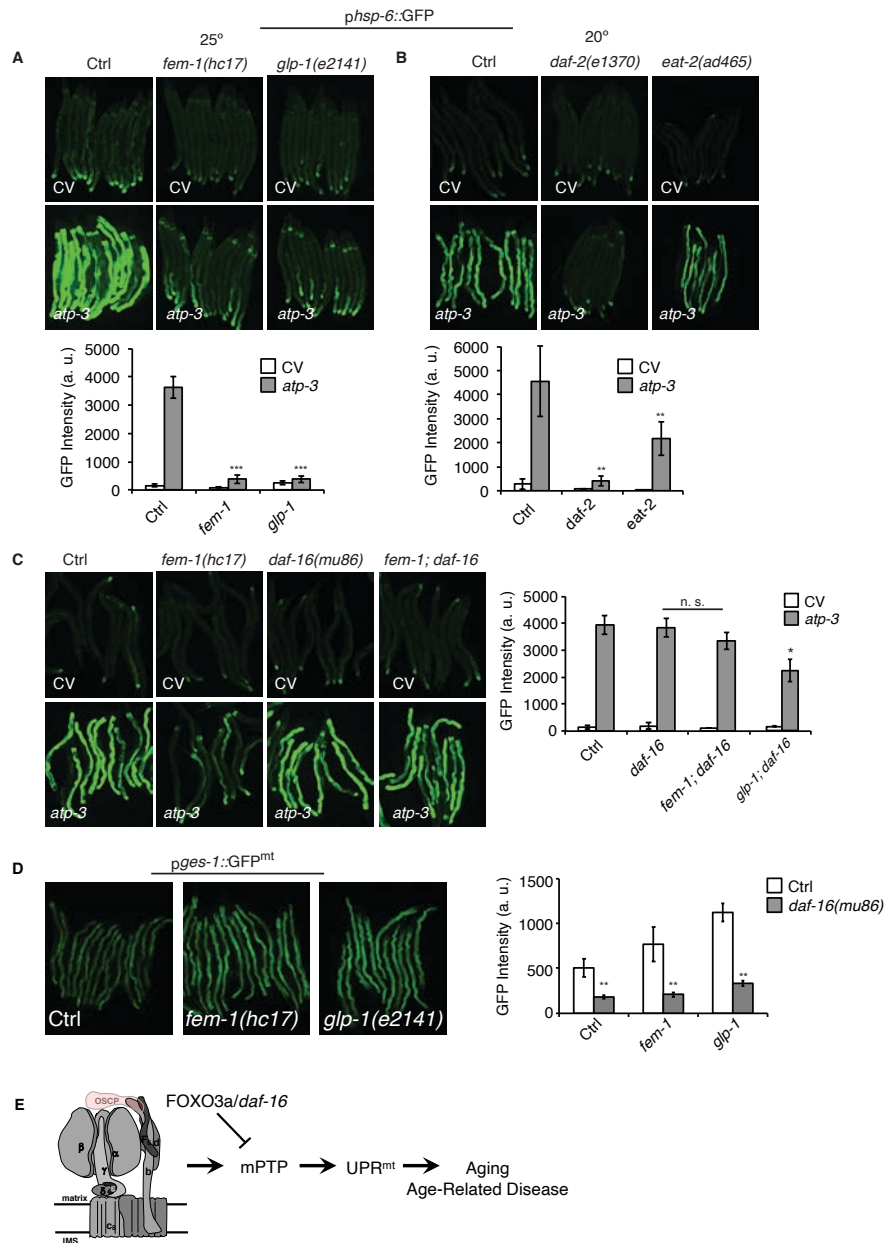
Figure 5: Long-lived Mutants Suppress the Post-Developmental UPR^{mt} Via FOXO3a/*daf-16*

(A, B) Long-lived germline mutants with a p*hsp-6*::GFP reporter strain background do not initiate a robust pdvUPR^{mt} due to loss of OSCP/*atp-3* via RNAi compared to p*hsp-6*::GFP controls. RNAi was administered for 48 hours beginning at young adulthood. Temperature sensitive mutants *glp-1(e2141)* and *fem-1(hc17)* and controls were developed at 25°C to initiate sterility and shifted to 20°C and RNAi plates as young adults. Data are the mean ± SEM of ≤ 15 animals combined from three biological experiments. ** p ≤ .001, ***p ≤ .0001 by Student's *t*-test. CV, control vector RNAi.

(C) The pdvUPR^{mt} is fully restored in *fem-1(hc17); daf-16(mu86)* mutants and partially restored in *glp-1(e2141); daf-16(mu86)* mutants. Temperature sensitive mutants and controls were developed at 25°C to initiate sterility and shifted to 20°C and RNAi as young adults. Data are the mean ± SEM of ≤ 15 animals combined from three biological experiments. *p ≤ .01 by Student's *t*-test. CV, control vector RNAi.

(D) Germline mutants *fem-1(hc17)* and *glp-1(e2141)* with a p*ges-1*::GFP^{mt} reporter display enhanced intestinal mitochondrial content. Germline mutants with a *daf-16(mu86)* mutation no longer display enhanced intestinal mitochondria. Temperature sensitive mutants and controls were developed at 25°C to initiate sterility and shifted to 20°C and RNAi as young adults. Data are the mean ± SEM of ≤ 15 animals combined from three biological experiments. ** p ≤ .001 by Student's *t*-test.

(E) Model: Loss of OSCP/*atp-3* initiates the mPTP, leading to activation of a maladaptive UPR^{mt}, contributing to aging and age-related diseases. FOXO3a/*daf-16* protects the mitochondria and suppresses mitochondrial dysfunction.

12

observed significantly higher mitochondrial mass in the intestines of *glp-1(e2141)* and *fem-1(hc17)*, which was dependent on FOXO3a/*daf-16*. To determine if the increased mitochondrial content may be due to a block in mitophagy or autophagy, we examined mitochondrial content after RNAi of *pdr-1* (parkin homology) and *hlh-30* (TFEB homolog). RNAi of *pdr-1* or *hlh-30* significantly increased the mitochondrial content in *glp-1(e2141)* and *fem-1(hc17)* mutants, suggesting that a block in mitophagy/autophagy was not the responsible mechanism. Overall, these findings suggest that *glp-1(e2141)* and *fem-1(hc17)* mutants are protected from initiating a maladaptive mPTP/pdvUPR^{mt}, possibly due to enhanced mitochondrial biogenesis via FOXO3a/*daf-16*.

DISCUSSION

While loss of the ATP synthase subunit OSCP/*atp-3* during development leads to lasting activation of the UPR^{mt} and is associated with longevity (Dillin et al., 2002; Rea et al., 2007), we have discovered that loss of this subunit during adulthood induces the mPTP and activates a reversible and *atfs-1*-dependent UPR^{mt} (pdvUPR^{mt}). Furthermore, we observed that activation of the UPR^{mt} during adulthood helps drive aging. Suppression of the mPTP/UPR^{mt} via genetic or pharmacological interventions is protective. Similarly, long-lived mutants from various longevity paradigms dependent on FOXO3a/*daf-16* are protected from the mPTP/UPR^{mt} during adulthood. The fact that loss of other OXPHOS subunits or loss of membrane potential via FCCP are not capable of inducing the UPR^{mt} during adulthood suggests a specific activation of the UPR^{mt} due to the mPTP. In contrast, it does not appear that the UPR^{mt} is activated in response to the mPTP during development. Thus, loss of OXPHOS subunits can have drastically different effects depending on the life stage or cellular milieu of the organism and suppression of the UPR^{mt} can be beneficial.

While the mPTP detrimental role in health is well established, considerable evidence suggests that the UPR^{mt} contributes to health and longevity (Houtkooper et al., 2013; Merkwirth et al., 2016; Mouchiroud et al., 2013; Sorrentino et al., 2017). Activating the UPR^{mt} in neurons can activate protective cell non-autonomous signals and also epigenetically rewire *C. elegans* to live longer (Durieux et al., 2011; Merkwirth et al., 2016; Tian et al., 2016; Zhang et al., 2018). NAD+ boosters appear to activate the UPR^{mt} and contribute to longevity and ameliorate AD (Mouchiroud et al., 2013; Sorrentino et al., 2017). However, an unbiased screen that identified activators of the UPR^{mt} found no correlation between UPR^{mt} activation and longevity (Bennett et al., 2014) and constitutive activation of the UPR^{mt} in dopaminergic neurons lead to increased neurodegeneration (Martinez et al., 2017). Activation of the UPR^{mt} in our setting is distinct in that it is specifically linked to activation of the mPTP. Thus, it is possible that preemptively boosting the UPR^{mt} may ward of aging and disease while activation in a diseased setting may exacerbate conditions, akin to instances of inflammation in disease.

We propose a model in which loss of OSCP/*atp-3* induces a conformational change in F-ATP synthase that leads to pore formation and activation of the UPR^{mt} during adulthood but not during development (Figure 5D). Previous reports have shown that loss of OSCP increases susceptibility to Ca^{2+}-induced mPTP formation and that key residues within the OSCP are required to suppress the mPTP during conditions of low pH (Antoniel et al., 2018; Giorgio et al., 2013), suggesting that a functional and intact OSCP protects against pore formation. OSCP

levels have also been shown to decrease with age while concomitantly increasing its binding to amyloid β, suggesting that loss of OSCP destabilizes the remaining ATP synthase to increase pore formation (Beck et al., 2016b). However, it has also been shown that OSCP provides the binding site for cyclophilin D and thus it has been proposed to be critical in the formation of the mPTP (Giorgio et al., 2017). However, these findings have been contested as knock out studies of OSCP show that cyclophilin D still binds to ATP synthase and EM studies have identified a cyclophilin D structure positioned on peripheral stalk subunits lateral to the OSCP (Daum et al., 2013; He et al., 2017a). Thus, our findings support a model in which loss of OSCP/*atp-3* induces a conformation change that is favorable for cyclophilin binding to the remaining peripheral stalk proteins or to sites independent of the F-ATP synthase, leading to destabilization of ATP synthase, pore formation with a loss of membrane potential, and subsequent activation of the pdvUPR[mt].

The loss of OSCP/*atp-3* may also be more impactful than other subunits. Unlike other ATP synthase subunits, OSCP/*atp-3* is prominently accessible in the mitochondrial matrix and has a diverse set of binding partners, such as estradiol and p53, which can modulate ATP production (Bergeaud et al., 2013; Zheng and Ramirez, 1999). Its loss may induce a strong protein misfolding cascade, reminiscent of the He and Lemasters mPTP model first proposed in 2002 (He and Lemasters, 2002). In this model, it was proposed that exposure to activators of the mPTP, such as oxidants, causes protein misfolding of integral membrane proteins, thereby recruiting chaperones such as cyclophilin D to repair. If the protein misfolding is unable to be repaired, then Ca^{2+}, along with cyclophilin D, could catalyze pore formation in a CysA-dependent manner. Indeed, both paraquat and manganese have been shown to induce both the UPR[mt] and the mPTP in separate studies (Angeli et al., 2014; Costantini et al., 1995; Nargund et al., 2012; Rao and Norenberg, 2004). However, more research is needed to clarify the relationship between protein misfolding and the mPTP.

Despite mounting evidence implicating F-ATP synthase as the pore-forming component of the mPTP, this remains controversial. The Walker lab has systematically deleted nearly every subunit of ATP synthase in a cell model and showed that a pore still forms (Carroll et al., 2019; He et al., 2017a; He et al., 2017b), leading some groups to suggest that in the absence of an intact F-ATP synthase, smaller low conductance CysA-dependent pores distinct from the mPTP still form (Neginskaya et al., 2019). Other groups have proposed that the mPTP can be mediated by ANT, as well as a cyclophilin D binding structure, which supports a "multi-pore model", which would explain why deletion of putative pore components may still yield pore formation (Carraro et al., 2020; Karch et al., 2019).

AD and PD both display evidence of the mPTP and in some instances, elevated UPR[mt] profiles have also been observed (Beck et al., 2016a; Beck et al., 2016b; Ludtmann et al., 2018; Perez et al., 2018; Sorrentino et al., 2017), but the relationship between these two mitochondrial processes have not been fully explored. Ischemic reperfusion directly causes the mPTP but little is known about the UPR[mt] under these conditions. Establishing a clearer understanding of the relationship between the UPR[mt] and the mPTP in these disease states could result in the development of new therapeutics for these and related disorders.

14

ACKNOWLEDGEMENTS

AUTHOR CONTRIBUTIONS

Conceptualization, S.A., J.K.A., and G.J.L.; Methodology, S.A., J.K.A., G.J.L., and A.C.F.; Investigation, S.A., A.C.F., T.H.P., M.C., D.B. and A.A.S., Validation, S.A. and A.C.F.; Resources, A.A.G.; Writing −Original Draft, S.A., J.K.A., and G.J.L.; Visualization, S.A., Supervision, S.A., J.K.A, G.L., Funding Acquisition, J.K.A. and G.J.L.

DECLARATION OF INTEREST

G.J.L. is cofounder of GeroState alpha and declares no financial interest related to this work. A.A.G. is founder of Image Analyst MKII Software and declares a financial interest.

MATERIAL AND METHODS

KEY RESOURCES

Chemicals

Tetramethylrhodamine methyl ester (perchlorate) (TMRM)	Cayman Chemical	Item # 21437
Cyclosporin A	Cayman Chemical	Item # 12088
FK506 (Tacrolimus)	Cayman Chemical	Item # 10007965
FCCP (Trifluoromethoxy carbonylcyanide phenylhydrazone)	Cayman Chemical	Item # 15218
Antibodies		
Mouse monoclonal anti-GRP 75 (D9)	Santa Cruz Biotechnology	Cat# sc-133137
Mouse monoclonal anti-β Tubulin Antibody (D-10)	Santa Cruz Biotechnology	Cat# sc-5274
Mouse monoclonal anti-β-Actin (8H10D10)	Cell Signaling Technology	Cat# 3700
Mouse monoclonal anti- ATP5A1 Monoclonal Antibody (15H4C4)	Invitrogen	Cat# 43-9800
Mouse monoclonal anti-ATP Synthase beta Monoclonal Antibody (3D5AB1)	Invitrogen	Cat# A-21351
Mouse monoclonal anti-NDUFS3 Monoclonal Antibody (17D95)	Invitrogen	Cat# 43-9200
Experimental Models: Organisms/Strains		
C. *elegans*: N2 Bristol	Caenorhabditis Genetics Center	RRID:WB-STRAIN:N2_(anscestral)
C. *elegans*: SJ4100 (zcIs13[*hsp-6*p::GFP])	Caenorhabditis Genetics Center	RRID:WB-STRAIN:SJ4100
C. *elegans*: SJ4058 (zcIs9[*hsp-60*p::GFP + *lin-15(+)*])	Caenorhabditis Genetics Center	RRID:WB-STRAIN:SJ4058

C. *elegans*: SJ4005 (zcIs4[*hsp-4*p::GFP])	Caenorhabditis Genetics Center	RRID:WB-STRAIN:VC1099
C. *elegans*: CL2070 (dvIs[*hsp-16.2*p::GFP])	Caenorhabditis Genetics Center	RRID:WB-STRAIN:CL2070
C. *elegans*: KWN190 (rnyEx109[*nhx-2*p::D3cpv + *pha-1*(+)], *pha-1(e2123) III; him-5(e1490) V*)	Caenorhabditis Genetics Center	RRID:WB-STRAIN:KWN190
C. *elegans*: ZC376.7 *atfs-1(tm4525)*	National BioResource Project	N/A
C. *elegans*: PHX1826 (qIs48[*atp-3(syb1826)*/hT2[*bli-4(e937) let-?(q782)*]])	SunyBiotech	N/A
C. *elegans*: SJ4143 (zcIs17 [*ges-1*p::GFP(mt)])	Caenorhabditis Genetics Center	RRID:WB-STRAIN:SJ4143
C. *elegans*: GL347 (SJ4100 (zcIs13[*hsp-6*p::GFP]) BC 6x to N2 Bristol)	This Study	N/A

CONTACT FOR REAGENT AND RESOURCE SHARING

Further information and requests for resources and reagents should be directed to and will be fulfilled by the Lead Contacts, Gordon Lithgow, glithgow@buckinstitute.org, Julie Andersen, jandersen@buckinstitute.org, and Suzanne Angeli, sangeli@buckinstitute.org

EXPERIMENTAL MODEL AND SUBJECT DETAILS

Nematode Strains

The following strain was obtained from the National BioResource Project: *atfs-1(tm4525)*. The following strains were obtained from the *Caenorhabditis* Genetic Center (CGC): SJ4100 (zcIs13[*hsp-6*p::GFP]), SJ4058 (zcIs9[*hsp-60*p::GFP]), SJ4005 (zcIs4[*hsp-4*p::GFP]), CL2070 (dvIs[*hsp-16.2*p::GFP]), SJ4143 (zcls17 [*ges-1*p::GFP(mt)]), KWN190 ([*pha-1(e2123)* III]; [*him-5(e1490)* V]; rnyEx109), CF1880 [*daf-16(mu86)*], CL2070 (dvIs70[*hsp-16.2p*::GFP], [*rol-6*(su1006)]), SJ4005 (zcls4[*hsp-4*::GFP]), DA1116 [*eat-2(ad1116)*] and N2 Bristol (wild-type). The following strain, SJ4100 (zcIs13[*hsp-6*p::GFP]) was backcrossed 6 times to wild-type N2 to generate GL347, which was used for all *hsp-6*p::GFP experiments. BA17 [*fem-1(hc17)*] and CB4037 [*glp-1(e2141)*] were back-crossed 3 times with wild-type N2 to create GL355 and GL345 respectively and used for the strains generated in this study. The following crossed strains were created in the Lithgow Lab for this study: GL364 [*fem-1(hc17)*], (zcIs13[*hsp-6*p::GFP]); GL346 [*glp-1(e2141)*], (zcIs13[*hsp-6*p::GFP]); GL380 [*daf-2(el370)*], (zcIs13[*hsp-6*p::GFP]); GL384 [*eat-2(ad1116)*], (zcIs13[*hsp-6*p::GFP]); GL361 [*fem-1(hc17)*], (zcls17 [*ges-1*p::GFP(mt)]); GL362 [*glp-1(e2141)*], (zcls17 [*ges-1*p::GFP(mt)]); GL369 [*fem-1(hc17)*], (zcIs13[*hsp-6*p::GFP], [*daf-16(mu86)*]); GL365 [*glp-1(e2141)*], (zcIs13[*hsp-6*p::GFP], [*daf-16(mu86)*]); GL370 [*fem-1(hc17)*], [*daf-16(mu86)*]; GL396 [*glp-1(e2141)*], [*daf-16(mu86)*]; GL361 [*fem-1(hc17)*], (zcls17 [*ges-1*p::GFP(mt)]; GL351 [*daf-16(mu86)*], (zcls17 [*ges-1*p::GFP(mt)]); GL389 [*fem-1(hc17)*], (zcls17 [*ges-1*p::GFP(mt)], [*daf-16(mu86)*]); GL358 [*glp-1(e2141)*] (zcls17 [*ges-1*p::GFP(mt)]), [*daf-16(mu86)*]; GL376 [*fem-1(hc17)*], (zcls4[*hsp-4*::GFP]); GL336 [*glp-1(e2141)*], (zcls4[*hsp-4*::GFP]); GL397 [*fem-1(hc17)*], (dvIs70[*hsp-16.2p*::GFP], [*rol-6*(su1006)]); GL342 [*glp-1(e2141)*], (dvIs70[*hsp-16.2p*::GFP], [*rol-6*(su1006)]).

CRISPR-Cas9 strain
The translational *atp-3*p::ATP-3::GFP was generated by SunyBiotech (http://www.sunybiotech.com/) using CRISPR-Cas9. The strain PHX1826 *atp-3(syb1826)*/hT2[*bli-4(e937) let-?(q782)* qIs48] was verified by PCR sequencing. The sgRNA target site used is as follows:
Sg1: CCCTTGCCACCGCCATCTAAatt
Sg2:CCGCCATCTAAatttttcccaaa.

Nematode and Bacterial Culture Conditions
Nematodes were maintained on nematode growth medium (NGM) plates. NGM plates were seeded with *E. coli* OP50 obtained from CGC that was grown in LB broth at 37˚C for 18 hours shaking at 225 rpm. Plates with bacteria were dried for 48 hours before use.

For RNAi experiments, *E. coli* HT115 (DE3) bacteria obtained from the Ahringer and Vidal RNAi Library was used (Kamath et al., 2003; Rual et al., 2004). All RNAi clones were verified via sequencing (Eurofins™). RNAi plates were prepared by cooling NGM to 55˚C and supplementing with a final concentration of 50ug/ml carbenicillin and 1mM Isopropyl β- d-1-thiogalactopyranoside (IPTG). RNAi bacteria was inoculated with one colony of RNAi bacteria into LB with 50ug/ml carbenicillin and was grown shaking overnight for 18 hours at 37˚ at 225 rpm.

Post-Developmental Timing
To achieve synchronous nematode populations, day 1 adult nematodes were allowed to lay eggs for 2 hours on seeded NGM plates. For convenience, nematodes were developed at 25˚C on *E. coli* OP50 until worms were visibly past the L4 stage (loss of crescent) but not yet gravid, approximately 45 hours for wild-type (although the time it takes for the worms to reach the young adult stage varies by strain). Nematodes were shifted to 20˚C once they reached adulthood.

METHOD DETAILS

RNA Interference (RNAi) Treatment
For developmental treatments, synchronized eggs were moved onto plates seeded with RNAi bacteria and developed at 20˚C for 72 hours. Nematodes were then either collected for analysis or for lifespans, remained on RNAi bacteria for the remainder of their life for survival analysis. For post-developmental treatments, synchronized eggs were developed on plates with *E. coli* OP50 at 25˚C until the young adult stage and then transferred to RNAi plates at 20˚C. Nematodes were collected after 48 hours for analysis or for lifespans, moved onto *E. coli* OP50 for the remainder of their life.

Quantitative RT-PCR
Approximately 300 adult nematodes were collected; nematode pellets were resuspended in 300uL RNA Lysis Buffer and frozen. Pellets was thawed, vortexed, and snap frozen three times. Zymo Research Quick-RNA MiniPrep kit was used to extract RNA. The primers used for qPCR are as follows:
act-1, Forward: ACGACGAGTCCGGCCCATCC
act-1, Reverse: GAAAGCTGGTGGTGACGATGGTT

atp-1, Forward: GAAGGACAAATCTCCCCACA
atp-2, Reverse: CGCCACATTCTTCCTTTTTC
atp-3, Forward: GCCTAATTTCTTAATTTTGCAGGT
atp-3, Reverse: GAACCTGAATCGGGGTCTTC
atp-4, Forward: AATATGTTGCCTCCCGTGAT
atp-4, Reverse: GGAACAAAAACGTTCATTCG
atp-5, Forward: TCTTCGACGTGCCGACAA
atp-5, Reverse: AAATGGTAGGAGAGCGATAAGG
nuo-2, Forward: TGAAGTTGCTGAGCCAACAC
nuo-2, Reverse: TCCACACTAACAGAAAATGAGTCT
cco-1, Forward: TTTCGGCTATTGTTCGCATT
cco-1, Reverse: GCCGTCTTAGCAAGTTGAGC

Lifespans

Day 1 adult nematodes were allowed to lay eggs for 2 hours on seeded NGM plates to obtain a synchronous aging population. 5-fluoro-2-deoxyuridine (FUdR) was omitted from plates due to its potentially confounding effects (Angeli et al., 2013). Worms are transferred to freshly seeded bacterial plates every day for the first 7 days of adulthood and then as needed afterwards. Worms were scored as dead when they failed to respond to gentle prodding with a platinum wire. Worms that experienced matricide or bagging were censored.

Tetramethylrhodamine Methyl Ester (TMRM) Staining

Plates were prepared by spotting seeded NGM plates with a TMRM solution diluted in water to a final concentration of 0.1 μM in the plates. Water was used as a solvent control. Plates were allowed to dry for 24 hours before use. For developmental experiments, synchronized eggs were placed on plates for 72 hours and then nematodes were collected for analysis. For post-developmental experiments, young adult nematodes were placed on plates for 48 hours and then collected for analysis.

Cyclosporine A (CysA) Treatment

Plates were prepared by spotting seeded NGM plates with a CysA (stock solution in DMSO) solution diluted in 100% ethanol. Comparable amounts of DMSO and ethanol were used as solvent controls. Plates were allowed to dry for 24 hours before use. For developmental experiments, synchronized eggs were placed on plates for 72 hours and then nematodes were collected for analysis. For post-developmental experiments, young adult nematodes were placed on plates for 48 hours and then collected for analysis; for lifespans, worms were moved to regular NGM plates for the remainder of their life after 48 hours on drug-treated RNAi bacteria.

Microscopy

Worms were anesthetized with 2mM levamisole and mounted on 2% agarose pads on glass slides. Fluorescence micrographs of GFP and TMRM were taken using a Zeiss Imager A2 at 5x magnification with 600ms exposure using the ZEN software. GFP expression was enhanced using the brightness/contrast tool in Photoshop. The same parameters were used for all images.

Confocal micrographs of mitochondrially targeted GFP and the cytosolic calcium sensor D3cpv (Zhang et al., 2016) were taken using a Zeiss LSM780 laser scanning confocal microscope using a 63× Plan Apochromat NA1.4. To visualize outlines of mitochondria, Image Analyst MKII (Image Analyst Software, Novato, CA) was used. Selected rectangular regions of interest (ROI) from the worm intestine were segmented and converted to outlines by a modification of the "Segment mitochondria" pipeline. Emission ratio images of D3cpv were excited at 440nm and captured at 450-490nm and 520-560nm and analyzed in Image Analyst MKII. Images were Wiener filtered and the ratio of the 540nm over the 470nm channel, indicative of cytosolic calcium concertation was calculated, and showed in pseudo-color coding. Emission ratios were determined in ROIs in the posterior intestine by the Plot Ratio function.

Western Blot
Approximately 30 to 50 adult worms were collected in S-basal buffer. Supernatant was removed and nematodes were flash-frozen. Worms pellets were resuspended in 2% SDS sample buffer with 2.5% β–mercaptoethanol and samples were boiled for 10 minutes. Samples were subjected to SDS-PAGE using 4-12% SDS gels (Invitrogen™) and transferred to Immun-Blot PVDF Membrane (BIO-RAD™) using BIO-RAD™ western blot Criterion apparatus. Membranes were blocked with 5% non-fat dry milk blocking solution; concentrations for antibodies were 1:1000 for primary antibodies and 1:2000 for secondary antibodies.

QUANTIFICATION, STATISTICS, AND PREDICTION
Statistics
Significance between control and experimental groups was determined by using two-tailed Student's t test. Asterisks denote corresponding statistical significance *$p < 0.05$; **$p < 0.01$; ***$p < 0.0001$. Error bars were generated using the standard error of the mean (SEM), typically from three pooled biological replicates. Graphpad Prism 7™ was used to plot survival curves. Log Rank (Mantel Cox) test in Prism™ was used to determine significance between the control and experimental group.

GFP Quantification
GFP intensity of worms was quantified using Image J 1.52A. The 'integrated density' of GFP expression and length of worms was measured using Image J tools. Integrated Density value was normalized by number of worms and average length of worms. The final value is in arbitrary units.

Mitochondrial Targeting Prediction
Mitochondrial presequences were predicted using the MitoFates tool (Fukasawa et al., 2015).
REFERENCES

Alavian, K.N., Beutner, G., Lazrove, E., Sacchetti, S., Park, H.A., Licznerski, P., Li, H., Nabili, P., Hockensmith, K., Graham, M*., et al.* (2014). An uncoupling channel within the c-subunit ring of the F1FO ATP synthase is the mitochondrial permeability transition pore. Proceedings of the National Academy of Sciences of the United States of America *111*, 10580-10585.
Angeli, S., Barhydt, T., Jacobs, R., Killilea, D.W., Lithgow, G.J., and Andersen, J.K. (2014). Manganese disturbs metal and protein homeostasis in Caenorhabditis elegans. Metallomics *6*, 1816-1823.

Angeli, S., Klang, I., Sivapatham, R., Mark, K., Zucker, D., Bhaumik, D., Lithgow, G.J., and Andersen, J.K. (2013). A DNA synthesis inhibitor is protective against proteotoxic stressors via modulation of fertility pathways in Caenorhabditis elegans. Aging (Albany NY) *5*, 759-769.

Antoniel, M., Jones, K., Antonucci, S., Spolaore, B., Fogolari, F., Petronilli, V., Giorgio, V., Carraro, M., Di Lisa, F., Forte, M.*, et al.* (2018). The unique histidine in OSCP subunit of F-ATP synthase mediates inhibition of the permeability transition pore by acidic pH. EMBO Rep *19*, 257-268.

Azarashvili, T., Odinokova, I., Bakunts, A., Ternovsky, V., Krestinina, O., Tyynela, J., and Saris, N.E. (2014). Potential role of subunit c of F0F1-ATPase and subunit c of storage body in the mitochondrial permeability transition. Effect of the phosphorylation status of subunit c on pore opening. Cell Calcium *55*, 69-77.

Baines, C.P., Kaiser, R.A., Purcell, N.H., Blair, N.S., Osinska, H., Hambleton, M.A., Brunskill, E.W., Sayen, M.R., Gottlieb, R.A., Dorn, G.W.*, et al.* (2005). Loss of cyclophilin D reveals a critical role for mitochondrial permeability transition in cell death. Nature *434*, 658-662.

Baker, B.M., Nargund, A.M., Sun, T., and Haynes, C.M. (2012). Protective coupling of mitochondrial function and protein synthesis via the eIF2alpha kinase GCN-2. PLoS genetics *8*, e1002760.

Basso, E., Fante, L., Fowlkes, J., Petronilli, V., Forte, M.A., and Bernardi, P. (2005). Properties of the permeability transition pore in mitochondria devoid of Cyclophilin D. The Journal of biological chemistry *280*, 18558-18561.

Beck, J.S., Mufson, E.J., and Counts, S.E. (2016a). Evidence for Mitochondrial UPR Gene Activation in Familial and Sporadic Alzheimer's Disease. Curr Alzheimer Res *13*, 610-614.

Beck, S.J., Guo, L., Phensy, A., Tian, J., Wang, L., Tandon, N., Gauba, E., Lu, L., Pascual, J.M., Kroener, S.*, et al.* (2016b). Deregulation of mitochondrial F1FO-ATP synthase via OSCP in Alzheimer's disease. Nat Commun *7*, 11483.

Bennett, C.F., Vander Wende, H., Simko, M., Klum, S., Barfield, S., Choi, H., Pineda, V.V., and Kaeberlein, M. (2014). Activation of the mitochondrial unfolded protein response does not predict longevity in Caenorhabditis elegans. Nat Commun *5*, 3483.

Bergeaud, M., Mathieu, L., Guillaume, A., Moll, U.M., Mignotte, B., Le Floch, N., Vayssiere, J.L., and Rincheval, V. (2013). Mitochondrial p53 mediates a transcription-independent regulation of cell respiration and interacts with the mitochondrial F(1)F0-ATP synthase. Cell Cycle *12*, 2781-2793.

Bernardi, P., and Di Lisa, F. (2015). The mitochondrial permeability transition pore: molecular nature and role as a target in cardioprotection. J Mol Cell Cardiol *78*, 100-106.

Bonora, M., Bononi, A., De Marchi, E., Giorgi, C., Lebiedzinska, M., Marchi, S., Patergnani, S., Rimessi, A., Suski, J.M., Wojtala, A.*, et al.* (2013). Role of the c subunit of the FO ATP synthase in mitochondrial permeability transition. Cell Cycle *12*, 674-683.

Bonora, M., Morganti, C., Morciano, G., Pedriali, G., Lebiedzinska-Arciszewska, M., Aquila, G., Giorgi, C., Rizzo, P., Campo, G., Ferrari, R.*, et al.* (2017). Mitochondrial permeability transition involves dissociation of F1FO ATP synthase dimers and C-ring conformation. EMBO Rep *18*, 1077-1089.

Carraro, M., Carrer, A., Urbani, A., and Bernardi, P. (2020). Molecular nature and regulation of the mitochondrial permeability transition pore(s), drug target(s) in cardioprotection. J Mol Cell Cardiol *144*, 76-86.

Carraro, M., Giorgio, V., Sileikyte, J., Sartori, G., Forte, M., Lippe, G., Zoratti, M., Szabo, I., and Bernardi, P. (2014). Channel formation by yeast F-ATP synthase and the role of dimerization in the mitochondrial permeability transition. The Journal of biological chemistry *289*, 15980-15985.

Carroll, J., He, J., Ding, S., Fearnley, I.M., and Walker, J.E. (2019). Persistence of the permeability transition pore in human mitochondria devoid of an assembled ATP synthase. Proceedings of the National Academy of Sciences of the United States of America *116*, 12816-12821.

Costantini, P., Petronilli, V., Colonna, R., and Bernardi, P. (1995). On the effects of paraquat on isolated mitochondria. Evidence that paraquat causes opening of the cyclosporin A-sensitive permeability transition pore synergistically with nitric oxide. Toxicology *99*, 77-88.

Daum, B., Walter, A., Horst, A., Osiewacz, H.D., and Kuhlbrandt, W. (2013). Age-dependent dissociation of ATP synthase dimers and loss of inner-membrane cristae in mitochondria. Proceedings of the National Academy of Sciences of the United States of America *110*, 15301-15306.

Dillin, A., Hsu, A.L., Arantes-Oliveira, N., Lehrer-Graiwer, J., Hsin, H., Fraser, A.G., Kamath, R.S., Ahringer, J., and Kenyon, C. (2002). Rates of behavior and aging specified by mitochondrial function during development. Science (New York, NY *298*, 2398-2401.

Durieux, J., Wolff, S., and Dillin, A. (2011). The cell-non-autonomous nature of electron transport chain-mediated longevity. Cell *144*, 79-91.

Farina, F., Alberti, A., Breuil, N., Bolotin-Fukuhara, M., Pinto, M., and Culetto, E. (2008). Differential expression pattern of the four mitochondrial adenine nucleotide transporter ant genes and their roles during the development of Caenorhabditis elegans. Dev Dyn *237*, 1668-1681.

Fukasawa, Y., Tsuji, J., Fu, S.C., Tomii, K., Horton, P., and Imai, K. (2015). MitoFates: improved prediction of mitochondrial targeting sequences and their cleavage sites. Mol Cell Proteomics *14*, 1113-1126.

Gauba, E., Guo, L., and Du, H. (2017). Cyclophilin D Promotes Brain Mitochondrial F1FO ATP Synthase Dysfunction in Aging Mice. J Alzheimers Dis *55*, 1351-1362.

Giorgio, V., Burchell, V., Schiavone, M., Bassot, C., Minervini, G., Petronilli, V., Argenton, F., Forte, M., Tosatto, S., Lippe, G., *et al.* (2017). Ca(2+) binding to F-ATP synthase beta subunit triggers the mitochondrial permeability transition. EMBO Rep *18*, 1065-1076.

Giorgio, V., von Stockum, S., Antoniel, M., Fabbro, A., Fogolari, F., Forte, M., Glick, G.D., Petronilli, V., Zoratti, M., Szabo, I., *et al.* (2013). Dimers of mitochondrial ATP synthase form the permeability transition pore. Proceedings of the National Academy of Sciences of the United States of America *110*, 5887-5892.

Goncalves, I.O., Passos, E., Diogo, C.V., Rocha-Rodrigues, S., Santos-Alves, E., Oliveira, P.J., Ascensao, A., and Magalhaes, J. (2016). Exercise mitigates mitochondrial permeability transition pore and quality control mechanisms alterations in nonalcoholic steatohepatitis. Appl Physiol Nutr Metab *41*, 298-306.

Guo, L., Carraro, M., Carrer, A., Minervini, G., Urbani, A., Masgras, I., Tosatto, S.C.E., Szabo, I., Bernardi, P., and Lippe, G. (2019). Arg-8 of yeast subunit e contributes to the stability of F-ATP synthase dimers and to the generation of the full-conductance mitochondrial megachannel. The Journal of biological chemistry *294*, 10987-10997.

Guo, Y., Zhang, K., Gao, X., Zhou, Z., Liu, Z., Yang, K., Huang, K., Yang, Q., and Long, Q. (2020). Sustained oligomycin sensitivity conferring protein expression in cardiomyocytes protects against cardiac hypertrophy induced by pressure-overload via improving mitochondrial function. Hum Gene Ther.

Haynes, C.M., Yang, Y., Blais, S.P., Neubert, T.A., and Ron, D. (2010). The matrix peptide exporter HAF-1 signals a mitochondrial UPR by activating the transcription factor ZC376.7 in C. elegans. Molecular cell *37*, 529-540.

He, J., Carroll, J., Ding, S., Fearnley, I.M., and Walker, J.E. (2017a). Permeability transition in human mitochondria persists in the absence of peripheral stalk subunits of ATP synthase. Proceedings of the National Academy of Sciences of the United States of America *114*, 9086-9091.

He, J., Ford, H.C., Carroll, J., Ding, S., Fearnley, I.M., and Walker, J.E. (2017b). Persistence of the mitochondrial permeability transition in the absence of subunit c of human ATP synthase. Proceedings of the National Academy of Sciences of the United States of America *114*, 3409-3414.

He, L., and Lemasters, J.J. (2002). Regulated and unregulated mitochondrial permeability transition pores: a new paradigm of pore structure and function? FEBS Lett *512*, 1-7.

Houtkooper, R.H., Mouchiroud, L., Ryu, D., Moullan, N., Katsyuba, E., Knott, G., Williams, R.W., and Auwerx, J. (2013). Mitonuclear protein imbalance as a conserved longevity mechanism. Nature *497*, 451-457.

Hsin, H., and Kenyon, C. (1999). Signals from the reproductive system regulate the lifespan of C. elegans. Nature *399*, 362-366.

Iurlaro, R., and Munoz-Pinedo, C. (2016). Cell death induced by endoplasmic reticulum stress. FEBS J *283*, 2640-2652.

Kamath, R.S., Fraser, A.G., Dong, Y., Poulin, G., Durbin, R., Gotta, M., Kanapin, A., Le Bot, N., Moreno, S., Sohrmann, M.*, et al.* (2003). Systematic functional analysis of the Caenorhabditis elegans genome using RNAi. Nature *421*, 231-237.

Karch, J., Bround, M.J., Khalil, H., Sargent, M.A., Latchman, N., Terada, N., Peixoto, P.M., and Molkentin, J.D. (2019). Inhibition of mitochondrial permeability transition by deletion of the ANT family and CypD. Sci Adv *5*, eaaw4597.

Kenyon, C., Chang, J., Gensch, E., Rudner, A., and Tabtiang, R. (1993). A C. elegans mutant that lives twice as long as wild type. Nature *366*, 461-464.

Kim, H.E., Grant, A.R., Simic, M.S., Kohnz, R.A., Nomura, D.K., Durieux, J., Riera, C.E., Sanchez, M., Kapernick, E., Wolff, S.*, et al.* (2016). Lipid Biosynthesis Coordinates a Mitochondrial-to-Cytosolic Stress Response. Cell *166*, 1539-1552 e1516.

Kokoszka, J.E., Waymire, K.G., Levy, S.E., Sligh, J.E., Cai, J., Jones, D.P., MacGregor, G.R., and Wallace, D.C. (2004). The ADP/ATP translocator is not essential for the mitochondrial permeability transition pore. Nature *427*, 461-465.

Labbadia, J., and Morimoto, R.I. (2015). Repression of the Heat Shock Response Is a Programmed Event at the Onset of Reproduction. Molecular cell *59*, 639-650.

Lin, Y.F., Schulz, A.M., Pellegrino, M.W., Lu, Y., Shaham, S., and Haynes, C.M. (2016). Maintenance and propagation of a deleterious mitochondrial genome by the mitochondrial unfolded protein response. Nature *533*, 416-419.

Liu, J., Farmer, J.D., Jr., Lane, W.S., Friedman, J., Weissman, I., and Schreiber, S.L. (1991). Calcineurin is a common target of cyclophilin-cyclosporin A and FKBP-FK506 complexes. Cell *66*, 807-815.

Ludtmann, M.H.R., Angelova, P.R., Horrocks, M.H., Choi, M.L., Rodrigues, M., Baev, A.Y., Berezhnov, A.V., Yao, Z., Little, D., Banushi, B., *et al.* (2018). alpha-synuclein oligomers interact with ATP synthase and open the permeability transition pore in Parkinson's disease. Nat Commun *9*, 2293.

Martinez, B.A., Petersen, D.A., Gaeta, A.L., Stanley, S.P., Caldwell, G.A., and Caldwell, K.A. (2017). Dysregulation of the Mitochondrial Unfolded Protein Response Induces Non-Apoptotic Dopaminergic Neurodegeneration in C. elegans Models of Parkinson's Disease. J Neurosci *37*, 11085-11100.

Merkwirth, C., Jovaisaite, V., Durieux, J., Matilainen, O., Jordan, S.D., Quiros, P.M., Steffen, K.K., Williams, E.G., Mouchiroud, L., Tronnes, S.U., *et al.* (2016). Two Conserved Histone Demethylases Regulate Mitochondrial Stress-Induced Longevity. Cell *165*, 1209-1223.

Mnatsakanyan, N., and Jonas, E.A. (2020). ATP synthase c-subunit ring as the channel of mitochondrial permeability transition: Regulator of metabolism in development and degeneration. J Mol Cell Cardiol *144*, 109-118.

Mnatsakanyan, N., Llaguno, M.C., Yang, Y., Yan, Y., Weber, J., Sigworth, F.J., and Jonas, E.A. (2019). A mitochondrial megachannel resides in monomeric F1FO ATP synthase. Nat Commun *10*, 5823.

Mouchiroud, L., Houtkooper, R.H., Moullan, N., Katsyuba, E., Ryu, D., Canto, C., Mottis, A., Jo, Y.S., Viswanathan, M., Schoonjans, K., *et al.* (2013). The NAD(+)/Sirtuin Pathway Modulates Longevity through Activation of Mitochondrial UPR and FOXO Signaling. Cell *154*, 430-441.

Munch, C., and Harper, J.W. (2016). Mitochondrial unfolded protein response controls matrix pre-RNA processing and translation. Nature *534*, 710-713.

Murphy, B.J., Klusch, N., Langer, J., Mills, D.J., Yildiz, O., and Kuhlbrandt, W. (2019). Rotary substates of mitochondrial ATP synthase reveal the basis of flexible F1-Fo coupling. Science (New York, NY *364*.

Nakagawa, T., Shimizu, S., Watanabe, T., Yamaguchi, O., Otsu, K., Yamagata, H., Inohara, H., Kubo, T., and Tsujimoto, Y. (2005). Cyclophilin D-dependent mitochondrial permeability transition regulates some necrotic but not apoptotic cell death. Nature *434*, 652-658.

Naresh, N.U., and Haynes, C.M. (2019). Signaling and Regulation of the Mitochondrial Unfolded Protein Response. Cold Spring Harb Perspect Biol *11*.

Nargund, A.M., Pellegrino, M.W., Fiorese, C.J., Baker, B.M., and Haynes, C.M. (2012). Mitochondrial import efficiency of ATFS-1 regulates mitochondrial UPR activation. Science (New York, NY *337*, 587-590.

Neginskaya, M.A., Solesio, M.E., Berezhnaya, E.V., Amodeo, G.F., Mnatsakanyan, N., Jonas, E.A., and Pavlov, E.V. (2019). ATP Synthase C-Subunit-Deficient Mitochondria Have a Small Cyclosporine A-Sensitive Channel, but Lack the Permeability Transition Pore. Cell Rep *26*, 11-17 e12.

Nicolli, A., Basso, E., Petronilli, V., Wenger, R.M., and Bernardi, P. (1996). Interactions of cyclophilin with the mitochondrial inner membrane and regulation of the permeability transition pore, and cyclosporin A-sensitive channel. The Journal of biological chemistry *271*, 2185-2192.

Ong, S.B., Samangouei, P., Kalkhoran, S.B., and Hausenloy, D.J. (2015). The mitochondrial permeability transition pore and its role in myocardial ischemia reperfusion injury. J Mol Cell Cardiol *78*, 23-34.

Panel, M., Ghaleh, B., and Morin, D. (2018). Mitochondria and aging: A role for the mitochondrial transition pore? Aging cell *17*, e12793.

Panowski, S.H., Wolff, S., Aguilaniu, H., Durieux, J., and Dillin, A. (2007). PHA-4/Foxa mediates diet-restriction-induced longevity of C. elegans. Nature *447*, 550-555.

Perez, M.J., Ponce, D.P., Aranguiz, A., Behrens, M.I., and Quintanilla, R.A. (2018). Mitochondrial permeability transition pore contributes to mitochondrial dysfunction in fibroblasts of patients with sporadic Alzheimer's disease. Redox Biol *19*, 290-300.

Rao, K.V., and Norenberg, M.D. (2004). Manganese induces the mitochondrial permeability transition in cultured astrocytes. The Journal of biological chemistry *279*, 32333-32338.

Rea, S.L., Ventura, N., and Johnson, T.E. (2007). Relationship between mitochondrial electron transport chain dysfunction, development, and life extension in Caenorhabditis elegans. PLoS biology *5*, e259.

Rolland, S.G., Schneid, S., Schwarz, M., Rackles, E., Fischer, C., Haeussler, S., Regmi, S.G., Yeroslaviz, A., Habermann, B., Mokranjac, D*., et al.* (2019). Compromised Mitochondrial Protein Import Acts as a Signal for UPR(mt). Cell Rep *28*, 1659-1669 e1655.

Rottenberg, H., and Hoek, J.B. (2017). The path from mitochondrial ROS to aging runs through the mitochondrial permeability transition pore. Aging cell *16*, 943-955.

Rual, J.F., Ceron, J., Koreth, J., Hao, T., Nicot, A.S., Hirozane-Kishikawa, T., Vandenhaute, J., Orkin, S.H., Hill, D.E., van den Heuvel, S*., et al.* (2004). Toward improving Caenorhabditis elegans phenome mapping with an ORFeome-based RNAi library. Genome Res *14*, 2162-2168.

Sorrentino, V., Romani, M., Mouchiroud, L., Beck, J.S., Zhang, H., D'Amico, D., Moullan, N., Potenza, F., Schmid, A.W., Rietsch, S*., et al.* (2017). Enhancing mitochondrial proteostasis reduces amyloid-beta proteotoxicity. Nature *552*, 187-193.

Takahashi, N., Hayano, T., and Suzuki, M. (1989). Peptidyl-prolyl cis-trans isomerase is the cyclosporin A-binding protein cyclophilin. Nature *337*, 473-475.

Tian, Y., Garcia, G., Bian, Q., Steffen, K.K., Joe, L., Wolff, S., Meyer, B.J., and Dillin, A. (2016). Mitochondrial Stress Induces Chromatin Reorganization to Promote Longevity and UPR(mt). Cell *165*, 1197-1208.

Urbani, A., Giorgio, V., Carrer, A., Franchin, C., Arrigoni, G., Jiko, C., Abe, K., Maeda, S., Shinzawa-Itoh, K., Bogers, J.F.M*., et al.* (2019). Purified F-ATP synthase forms a Ca(2+)-dependent high-conductance channel matching the mitochondrial permeability transition pore. Nat Commun *10*, 4341.

Ye, X., Linton, J.M., Schork, N.J., Buck, L.B., and Petrascheck, M. (2014). A pharmacological network for lifespan extension in Caenorhabditis elegans. Aging cell *13*, 206-215.

Yoneda, T., Benedetti, C., Urano, F., Clark, S.G., Harding, H.P., and Ron, D. (2004). Compartment-specific perturbation of protein handling activates genes encoding mitochondrial chaperones. Journal of cell science *117*, 4055-4066.

Yung, H.W., Colleoni, F., Dommett, E., Cindrova-Davies, T., Kingdom, J., Murray, A.J., and Burton, G.J. (2019). Noncanonical mitochondrial unfolded protein response impairs placental oxidative phosphorylation in early-onset preeclampsia. Proceedings of the National Academy of Sciences of the United States of America *116*, 18109-18118.

Zhang, F., Peng, D., Cheng, C., Zhou, W., Ju, S., Wan, D., Yu, Z., Shi, J., Deng, Y., Wang, F*., et al.* (2016). Bacillus thuringiensis Crystal Protein Cry6Aa Triggers Caenorhabditis elegans Necrosis Pathway Mediated by Aspartic Protease (ASP-1). PLoS pathogens *12*, e1005389.

Zhang, Q., Wu, X., Chen, P., Liu, L., Xin, N., Tian, Y., and Dillin, A. (2018). The Mitochondrial Unfolded Protein Response Is Mediated Cell-Non-autonomously by Retromer-Dependent Wnt Signaling. Cell *174*, 870-883 e817.

Zheng, J., and Ramirez, V.D. (1999). Purification and identification of an estrogen binding protein from rat brain: oligomycin sensitivity-conferring protein (OSCP), a subunit of mitochondrial F0F1-ATP synthase/ATPase. J Steroid Biochem Mol Biol *68*, 65-75.

Zhou, B., Kreuzer, J., Kumsta, C., Wu, L., Kamer, K.J., Cedillo, L., Zhang, Y., Li, S., Kacergis, M.C., Webster, C.M.*, et al.* (2019). Mitochondrial Permeability Uncouples Elevated Autophagy and Lifespan Extension. Cell *177*, 299-314 e216.
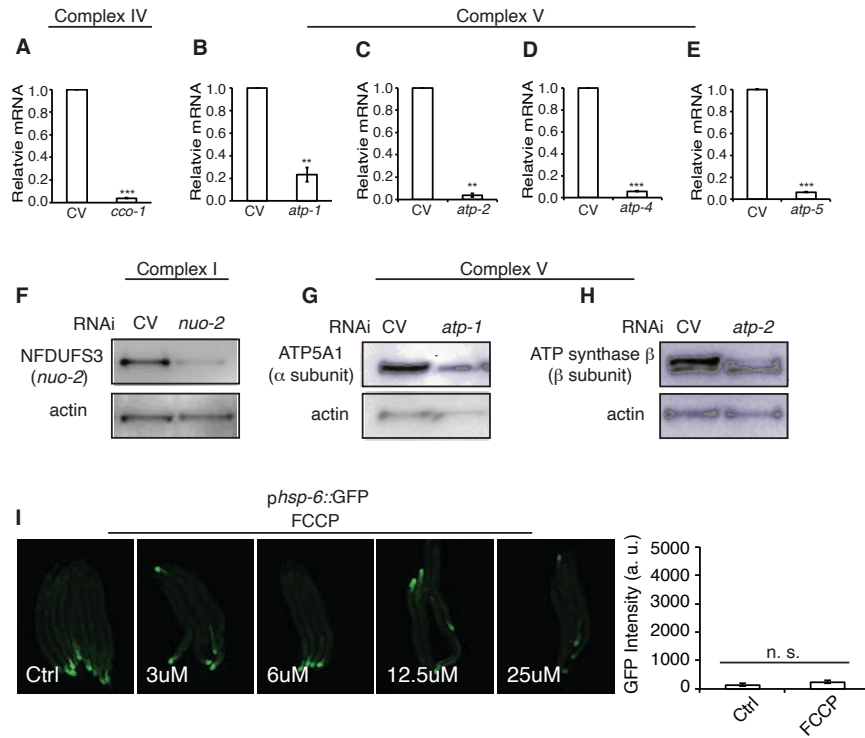
SUPPLEMENTAL FIGURES

Figure S1: RNAi Efficiency and FCCP in Young Adult *C. elegans*

(A-E) qRTPCR from N2 worms after RNAi of subunits from complex IV and V. RNAi was administered for 48 hours beginning at young adulthood. Data are the mean ± SD ≤ 150 animals combined from two experiments. **p ≤ 0.01, ***p ≤ .0001 by Student's *t*-test.

(F-H) Immunoblots from N2 worms after RNAi of subunits from complex I and V. RNAi was administered for 48 hours beginning at young adulthood. Representative immunoblots from two biological experiments. Actin was used as a loading control.

(I) Dose-response treatment with the mitochondrial uncoupler, FCCP, did not significantly induce the p*hsp-6*::GFP reporter. FCCP was administered for 24- 48 hours beginning at young adulthood. Data are the mean ± SEM of ≤ 15 animals from three biological experiments. n. s., not significant by Student's *t*-test.
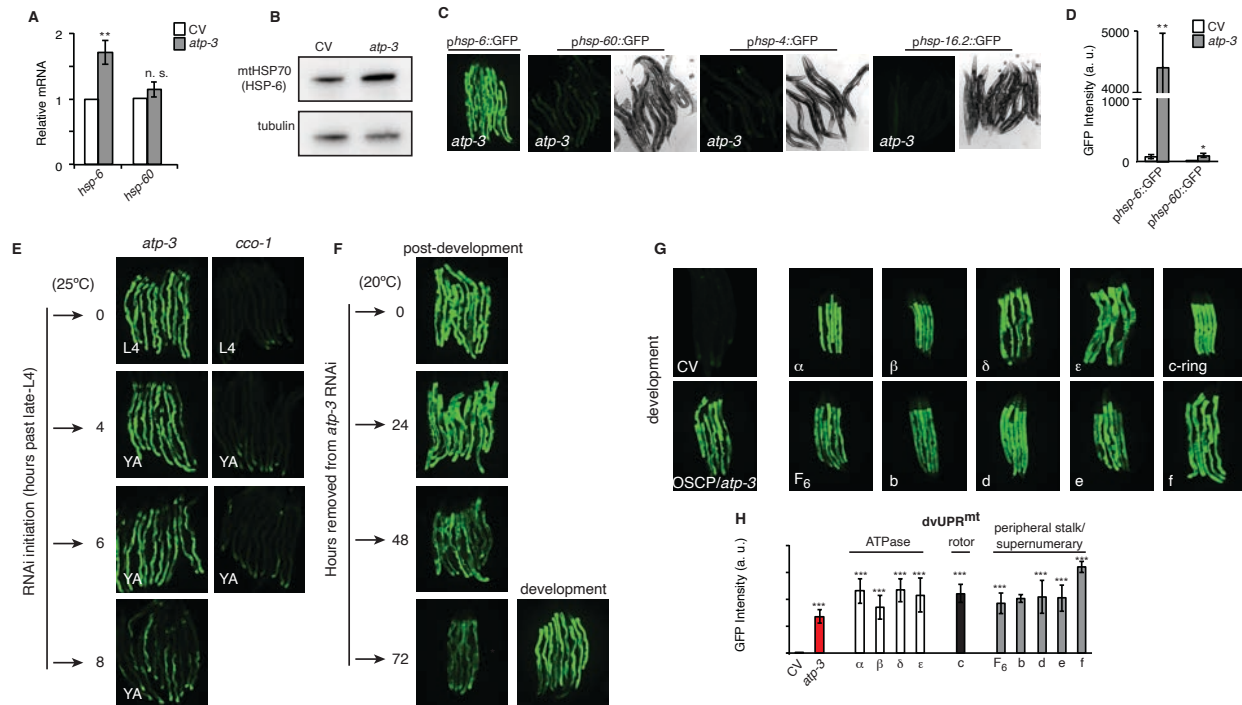
Figure S2: Loss of the ATP Synthase Subunit, OSCP/*atp-3*, Induces a Specific, Temporally Confined, and Reversible Post-Developmental UPR^{mt}

(A) qRTPCR of *hsp-6* and *hsp-60* from N2 worms on post-developmental CV or *atp-3* RNAi. Data are the mean ± SEM of ≤ 150 animals combined from four biological experiments. **p ≤ 0.01, n.s. not significant by Student's *t*-test. CV, control vector RNAi.

(B) Western blot of mtHSP70/HSP-6 and tubulin (loading control) from worms on post-developmental CV or *atp-3* RNAi. CV, control vector RNAi. Representative blot from three biological experiments.

(C) Post-developmental RNAi of *atp-3* mildly induced the mitochondrial p*hsp-60*::GFP reporter but not the UPR^{ER} p*hsp-4*::GFP or HSR p*hsp-16.2*::GFP reporters. Left panel, fluorescent channel; right panel, bright-field channel. CV, control vector RNAi.

(D) Quantification of p*hsp-6*::GFP and p*hsp-60*::GFP reporters from (A). Data are the mean ± SEM of ≤ 15 animals combined from three biological experiments. **p ≤ 0.01, *p ≤ 0.05 by Student's *t*-test.

(E) Post-developmental RNAi of *atp-3* or *cco-1* RNAi that was initiated at L4, young adult, and adult stages using the p*hsp-6*::GFP reporter at 25°C. GFP expression was assessed 48 hours after RNAi initiation. Representative pictures from two biological experiments.

(F) The p*hsp-6*::GFP reporter worms were treated with developmental or post-developmental *atp-3* RNAi. Worms were removed from HT115 RNAi bacteria and placed onto OP50 bacteria and GFP expression was assessed at indicated time-points. Representative pictures from two biological experiments.

(G) Developmental RNAi of all ATP synthase subunits tested induced the p*hsp-6*::GFP reporter. For developmental treatment, worms were exposed to RNAi beginning from eggs for 72 hours.

(H) Quantification of GFP intensity from (G). Data are the mean ± SEM of ≤ 15 animals combined from three biological experiments. ***p ≤ .0001 by Student's *t*-test. dv, development. See Table S3 for additional details.
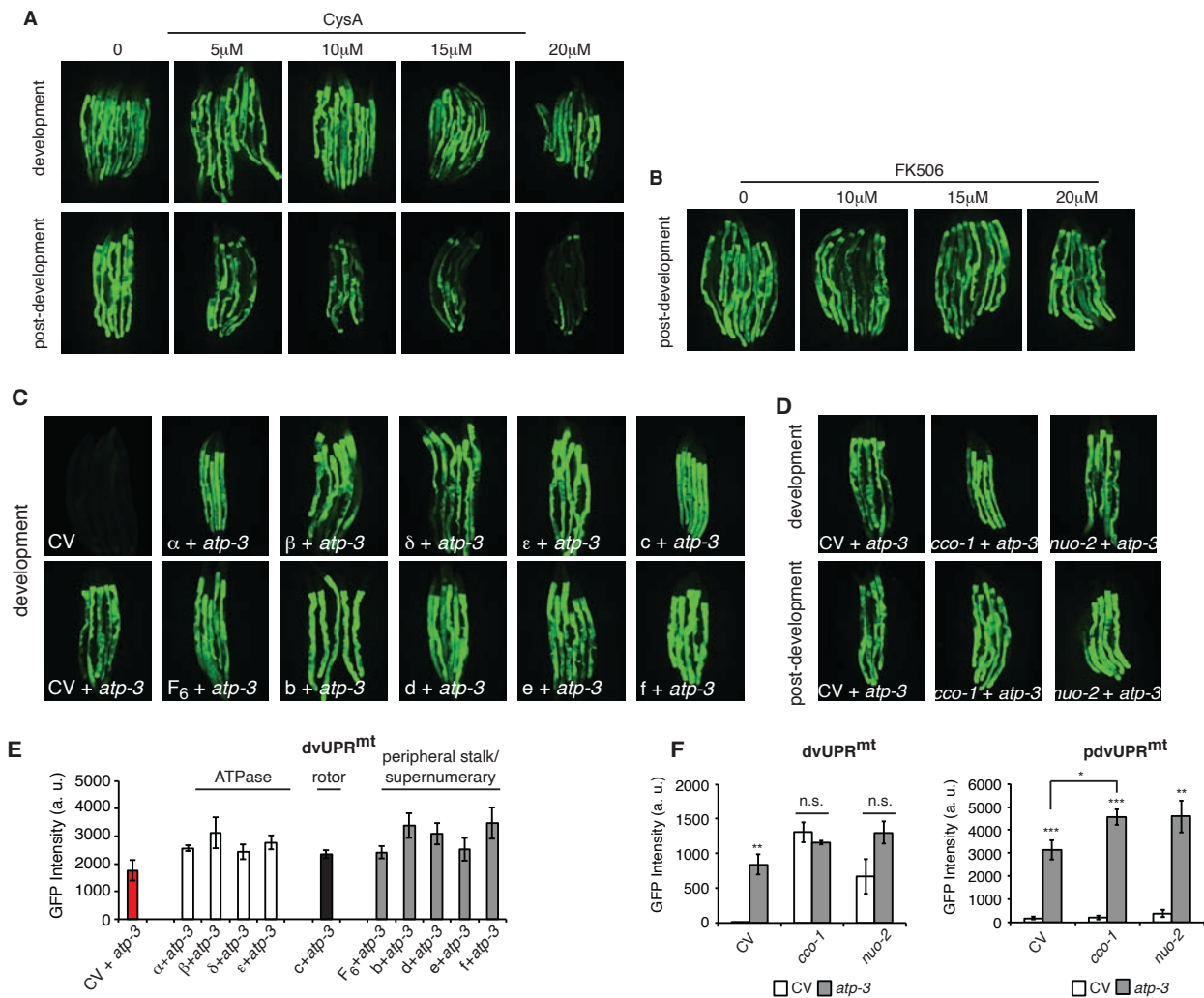
27

Figure S3: The Post-developmental but not Developmental UPR^{mt} is Modulated by the mPTP

(A) Dose response of CysA administered during development or post-development on *atp-3* RNAi-treated p*hsp-6*::GFP reporter worms.

(B) Dose response of FK506 administered during post-development on *atp-3* RNAi-treated p*hsp-6*::GFP reporter worms.

(C) Concomitant developmental RNAi of *atp-3* and individual ATP synthase subunits induced the p*hsp-6*::GFP reporter. For developmental treatment, worms were exposed to RNAi beginning from eggs for 72 hours.

(D) Concomitant developmental or post-developmental RNAi of *atp-3* and either *cco-1* or *nuo-2* induced the p*hsp-6*::GFP reporter.

(E, F) Quantification of GFP intensity from (C) and (D). Data are the mean ± SEM of ≤ 15 animals combined from three biological experiments. (E) No significant differences from CV + *atp-3* condition. ** p ≤ .0001, ***p ≤ .0001 by Student's *t*-test. dvUPR^{mt}, development; pdv, post-development.
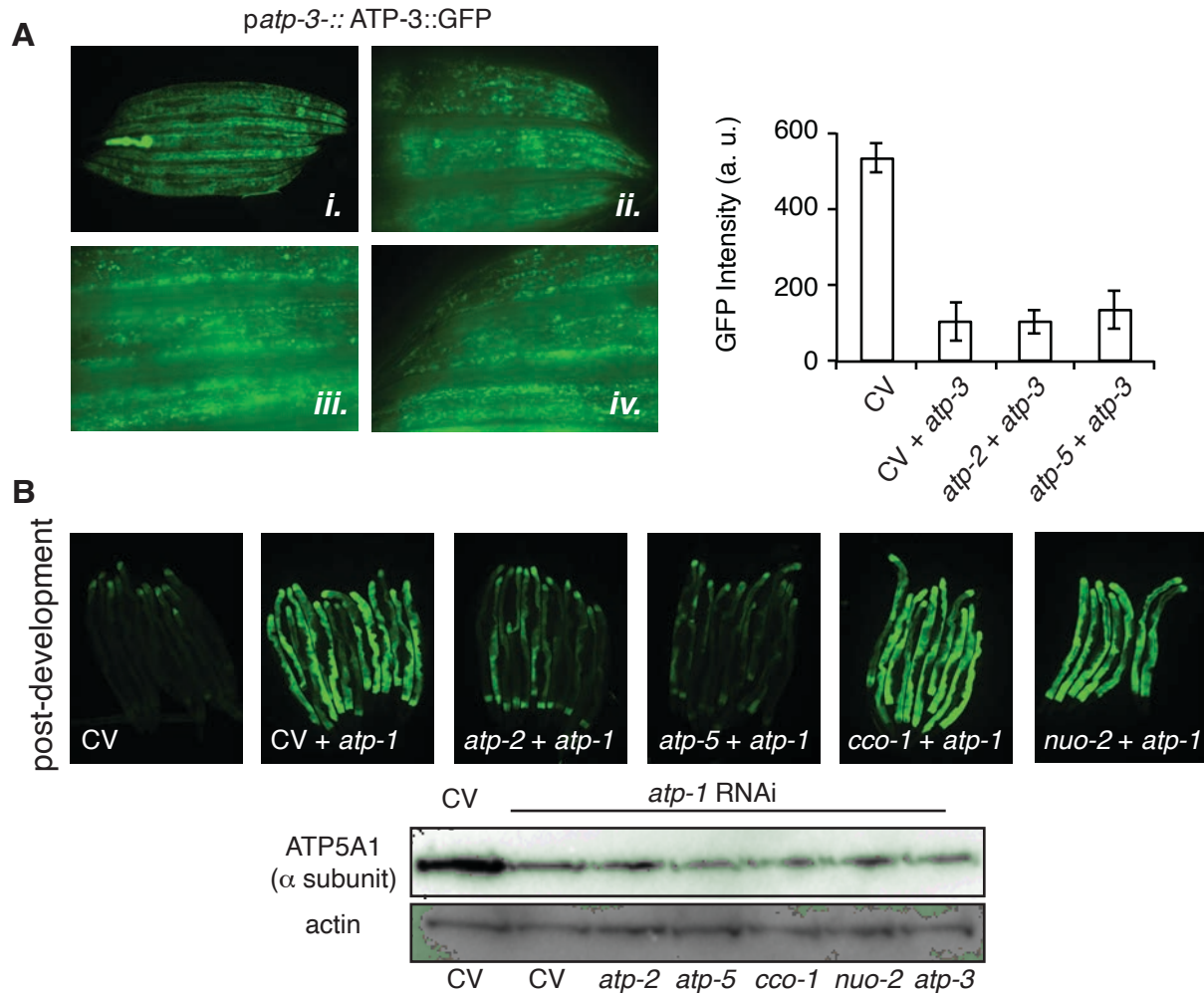
28

A

p*atp-3-::* ATP-3::GFP

B

Figure S4: Effects of Loss of OXPHOS Subunits on the dvUPR^{mt} and pdvUPR^{mt}

(A) Dual-RNAi effectively knocks down ATP-3 protein synthesis as measured by the translational p*atp-3*::ATP-3::GFP reporter, i.10X photomicrographs of homozygous and heterozygous (bright pharyngeal GFP expression) worms, ii. 40X photomicrographs of head region of control homozygous worms, iii. 40X photomicrographs of mid-region of control homozygous worms, iv. 40X photomicrographs of tail region of control homozygous worms.

(B) RNAi of *atp-1* induces a post-developmental UPR^{mt} similar to *atp-3* in the p*hsp-6*::GFP reporter. Representative results from two biological experiments. Immunoblot of ATP-1 from p*hsp-6*::GFP reporter worms after dual-RNAi treatment. Representative blots from two biological experiments.
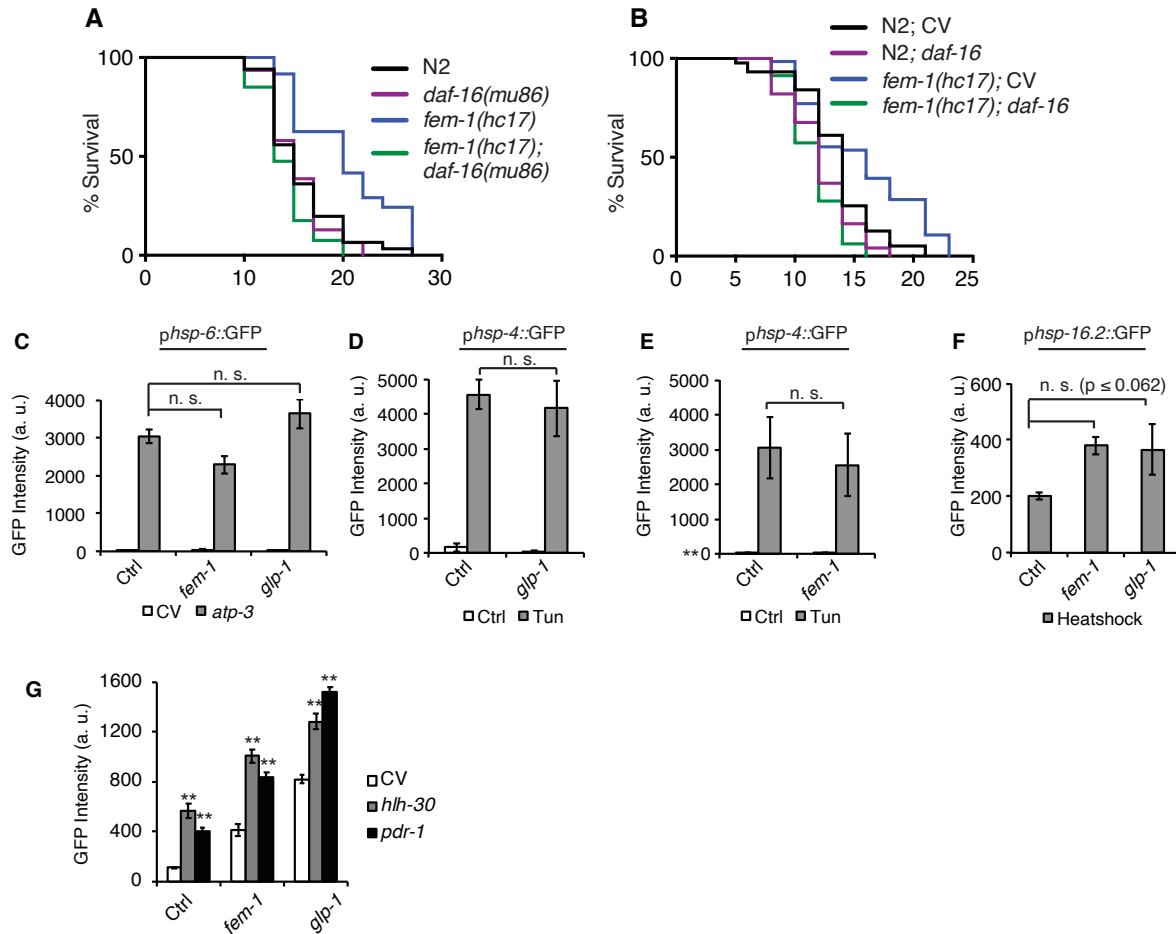
29

Figure S5: Characterization of germline mutant longevity, stress response, and mitophagy/autophagy processes.

(A) Germline mutant *fem-1(hc17)* is long-lived, which is abolished in *daf-16(mu86)* mutant background. Worms were developed at 25°C and shifted to 20°C beginning at young adulthood.

(B) Germline mutant *fem-1(hc17)* is long-lived, which is abolished after treatment with *daf-16* RNAi. Worms were developed at 25°C and shifted to 20°C beginning at young adulthood.

(C) Germline mutants *fem-1(hc17)* and *glp-1(e2141)* with a p*hsp-6*::GFP reporter strain background induce robust UPR^{mt} when OSCP/*atp-3* RNAi is administered during development. Worms were developed at 25°C and exposed to RNAi beginning from the egg stage and collected for microscopy after approximately 48 hours.

(D, E) Germline mutants *fem-1(hc17)* and *glp-1(e2141)* with a p*hsp-4*::GFP reporter strain background induce robust UPR^{ER} when exposed to 4ug/ml tunicamycin. Worms were developed at 25°C and exposed to tunicamycin as young adults and collected for microscopy after approximately 24 hours. Tunicamycin was spotted onto seeded NGM plates and water was used as the solvent control.

(F) Germline mutants *fem-1(hc17)* and *glp-1(e2141)* with a p*hsp-16.2*::GFP reporter strain background induce a robust heat-shock response when to 33°C for 2 hours. Worms were developed at 25°C and exposed to heat as young adults following immediate collection for microscopy.

(G) Germline mutants *fem-1(hc17)* and *glp-1(e2141)* with a p*ges-1*::GFP^{mt} reporter strain background exhibit higher intestinal mitochondrial mass after RNAi with *pdr-1* and *hlh-30*. Worms were developed at 25°C and shifted to 20°C and exposed to RNAi as young adults; worms were collected for microscopy after approximately 48 hours.

30

SUPPLEMENTAL TABLES

	gene	dvUPR^{mt}	pdvUPR^{mt}	pdvUPR^{mt} fold change	p-value
Complex I	*nuo-1*	yes	yes	2.6	0.0002
	nuo-2	yes	yes	2.1	0.0155
Complex III	*cyc-1*	yes	yes	2.1	< 0.0001
Complex IV	*cco-1*	yes	no	1.9	0.0511
Complex V	*atp-2*	yes	yes	2.7	0.0029
	atp-3	yes	yes	71.6	< 0.0001
Other	*clk-1*	yes	no	-1.5	0.0064
	mrps-5	yes	no	1.0	0.9671
	tomm-22	yes	no	-1.8	0.0004

Supplemental Table 1: List of genes tested for whether they induce a developmental UPR^{mt} (dvUPR^{mt}) or post-developmental UPR^{mt} (pdvUPR^{mt}).

Complex V	gene	subunit	dvUPR^{mt}	pdvUPR^{mt}	pdvUPR^{mt} fold change	p-value
F1 ATPase	atp-1	α	yes	yes	19.7	0.0004
F1 ATPase	atp-2	β	yes	yes	2.7	0.0029
F1 ATPase	F58F12.1	δ	yes	yes	1.5	0.0410
F1 ATPase	hpo-18	ε	yes	yes	12.3	< 0.0001
F1 peripheral stalk	atp-3	OSCP	yes	yes	55.4	< 0.0001
F1 peripheral stalk	asb-2	b	yes	no	1.9	0.0797
F1 peripheral stalk	atp-5	d	yes	no	1.1	0.6388
F1 peripheral stalk	atp-4	F6	yes	no	1.2	0.2206
Fo rotor	Y82E9BR.3	c	yes	yes	3.8	0.0003
Fo supernumerary	R04F11.2	e	yes	no	1.0	0.9604
Fo supernumerary	R53.4	f	yes	no	1.1	0.7152

Supplemental Table 2: Summary of the effects of RNAi of ATP synthase subunits on the developmental UPR^{mt} (dvUPR^{mt}) or post-developmental UPR^{mt} (pdvUPR^{mt}).

gene	MTS strength
cyn-1	0.941
cyn-2	0.0
cyn-3	0.0
cyn-4	0.0
cyn-5	0.0
cyn-6	0.0
cyn-7	0.0
cyn-8	0.0
cyn-9	0.0
cyn-10	0.0
cyn-11	0.0
cyn-12	0.0
cyn-13	0.0
cyn-14	0.0
cyn-15	0.0
cyn-16	0.0
cyn-17	0.154
atfs-1	0.117

Supplemental Table 3: List of *C. elegans* cyclophilins and their predicted mitochondrial localization using the MitoFates mitochondrial targeting sequence (MTS) prediction tool.

	Strain	Median lifespan (days)	Deaths/Events	Censored Animals	Deaths/Censored	p-value
Development	N2; cv	15	48	20	48/20	
	N2; *atp-3*	26.5	34	30	34/30	*** < 0.0001
	N2; cv	15	161	38	161/38	
Post-development	N2; *atp-3*	10	181	20	181/20	*** < 0.0001
	atfs-1; cv	12	117	63	117/63	
	atfs-1; atp-3	9	157	31	157/31	*** < 0.0001
	N2; cv	17	116	27	116/27	
	N2; *cyc-1*	17	137	22	137/22	0.6097
	N2; *cco-1*	17	139	6	139/6	0.2826
	N2; *atp-2*	15	131	22	131/22	** 0.0067
	N2; *nuo-2*	17	128	27	128/27	0.5893
Post-development	N2; cv	15	124	33	124/33	
	N2; *atp-3*	13	130	16	130/16	*** < 0.0001
	N2; cv 15uM CysA	17	85	24	85/24	
	N2; *atp-3* 15uM CysA	17	112	35	112/35	0.6084

Supplemental Table 4: Summary of lifespans.